Basin Research (2008) **20**, 305–331, doi: 10.1111/j.1365-2117.2007.00346.x

Trench-forearc interactions reflected in the sedimentary fill of Talara basin, northwest Peru

Andrea Fildani,[1] Angela M. Hessler and Stephan A. Graham

Department of Geological and Environmental Sciences, Stanford University, Stanford, CA, USA

ABSTRACT

Exceptional exposure of the forearc region of NW Peru offers insight into evolving convergent margins. The sedimentary fill of the Talara basin spans the Cretaceous to the Eocene for an overall thickness of 9000 m and records within its stratigraphy the complicated history of plate interactions, subduction tectonics, terrane accretion, and Andean orogeny. By the early Tertiary, extensional tectonism was forming a complex horst and graben system that partitioned the basin into a series of localized depocentres. Eocene strata record temporal transitions from deltaic and fluvial to deep-water depositional environments as a response to abrupt, tectonically controlled relative sea-level changes across those depocentres. Stratigraphic and provenance data suggest a direct relationship between sedimentary packaging and regional tectonics, marked by changes in source terranes at major unconformities. A sharp shift is recognized at the onset of deepwater (bathyal) sedimentation of the Talara Formation, whose sediments reflect an increased influx of mafic material to the basin, likely related to the arc region. Although the modern topography of the Amotape Mountains partially isolates the Talara basin from the Lancones basin and the Andean Cordillera to the east, provenance data suggest that the Amotape Mountains were not always an obstacle for Cordilleran sediment dispersal. The mountain belt intermittently isolated the Talara basin from Andean-related sediment throughout the early Tertiary, allowing arc-related sediment to reach the basin only during periods of subsidence in the forearc region, probably related to plate rearrangement and/or seamounts colliding with the trench. Intraplate coupling and/or partial locking of subduction plates could be among the major causes behind shifts from contraction to extension (and enhanced subduction erosion) in the forearc region. Eventually, collisional tectonic and terrane accretion along the Ecuadorian margin forced a major late-Eocene change in sediment dispersal.

INTRODUCTION

Forearc basins record compelling evidence about the age, nature and intensity of subduction-related tectonic events (Dickinson, 1995). Forearc basin sedimentary fills have low preservation potential because many active margins involve accretionary phases with major shortening and/or destructive phases (i.e. subduction erosion). The Mesozoic forearc is missing in most of southern Peru, and as much as 148 km in width of the South American margin has been lost since the Eocene at the Lima basin latitude because of subduction erosion (Clift *et al.*, 2003). However, in NW Peru, approximately 9000 m of near-continuous forearc sedimentation preserved in the Talara basin (Figs 1 and 2) records events occurring at a dynamic Andean juncture: between (1) active ridge subduction (Witt *et al.*, 2006) and terrane accretion (Spikings *et al.*, 2005) to the north and (2) an area of active subduction erosion to the south (Lima basin: Clift *et al.*, 2003).

The Peru-Chile arc-trench system extends for more than 5000 km along the western margin of South America, where subduction of the oceanic Nazca plate at a rate of about 6–7 cm year^{-1} has formed a series of forearc basins (Clift *et al.*, 2003; Witt *et al.*, 2006; Figs 1 and 2). Despite convergence across the interface between the South America and Nazca plates, extensional events are common along the Peruvian and Ecuadorian margins (Clift *et al.*, 2003; Sage *et al.*, 2006; Witt *et al.*, 2006). In the region of Talara, a series of extensional events accommodated nearly continuous sedimentary in-filling from the Late Cretaceous to the Neogene (Jaillard *et al.*, 2000) (Fig. 3), with subsidence controlled by normal faulting and large-scale detachment faults. Horst and graben structures fostered thick sediment accumulation and abrupt lateral facies variations, with loci of deep-water sedimentation developing in the middle and late Eocene (Fildani, 2004; Duerichen, 2005). Basin inversion began in the late Oligocene (Seranne, 1987) and continued through the Neogene (Noblet *et al.*, 1996). Ridge collision and partial subduction (well

Correspondence: Andrea Fildani, Department of Geological and Environmental Sciences, Stanford University, Stanford, CA 94305, USA. E-mail: andreafildani@chevron.com

[1] Present address: Chevron Energy and Technology Company, 6001 Bollinger Canyon Rd., Rm. D1192, San Ramon, CA 94583, USA.

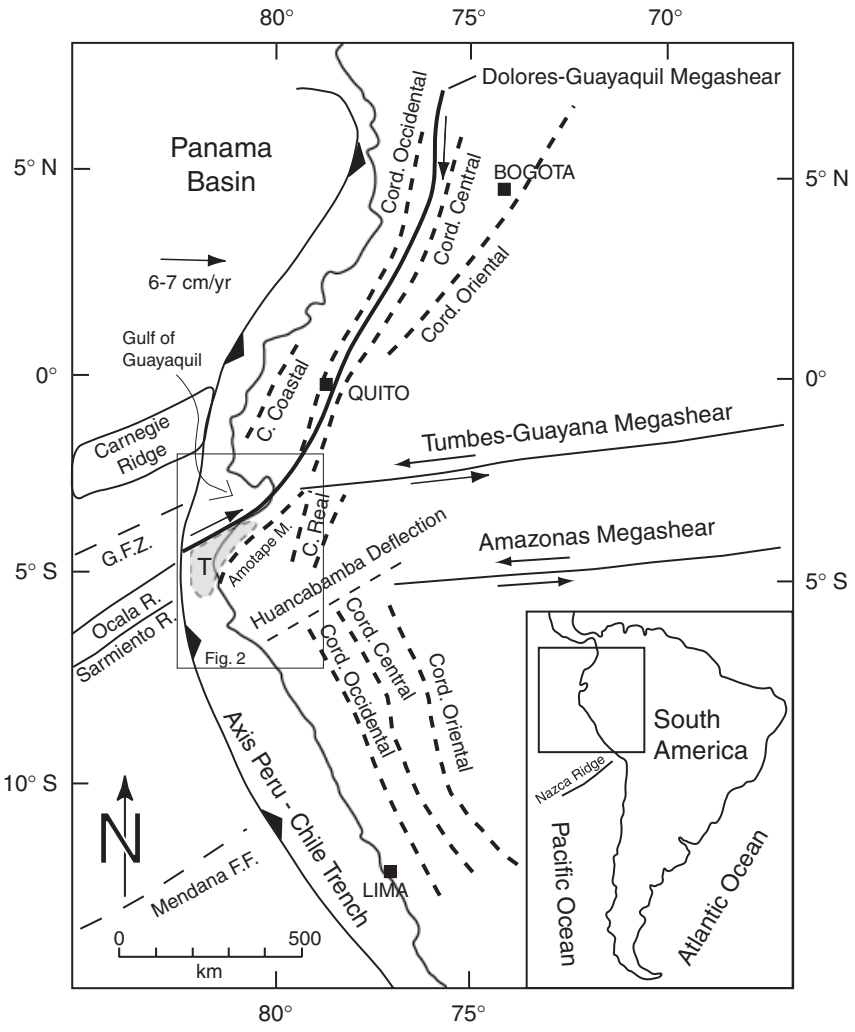

Fig. 1. Distribution of major tectonic lineaments of the northern Andes, and of the Peru–Chile Trench with intersecting seamount chains. Location of Talara basin is in grey and marked with a T, G.F.Z., Grijalba Fracture Zone. C. Real, Cordillera Real. The Nazca Ridge location is reported in the inset map (map modified from Shepherd & Moberly, 1981).

documented to the north of the study area, i.e. Carnegie ridge; Fig. 1) is presumed responsible for the uplift and exhumation of most of the Ecuador and northern Peru coastline (Gutscher *et al.*, 1999a; Pedoja *et al.*, 2006; Witt *et al.*, 2006).

This paper focuses on the sedimentary record in the onshore part of the basin, where the sedimentary fill consists of 60–70% shale, with the balance being sandstone and conglomerate. The purpose of this study is three-fold: (1) to re-evaluate the stratigraphic record of the Talara basin based on evolving depositional environments, (2) to determine the provenance of distinctive sedimentological cycles of the basin and (3) to evaluate large-scale tectonic implications for the northern Central Andes. We use stratigraphic stacking patterns, sediment dispersal patterns, sandstone petrography, mudstone geochemistry, and conglomerate clast data to relate local forearc development to large-scale subduction processes, such as seamount subduction (Gutscher *et al.*, 1999a, b; Witt *et al.*, 2006), subduction erosion (Clift *et al.*, 2003; Laursen & Normark, 2003), accretionary tectonics (Spikings *et al.*, 2005), and changes in plate convergence rate (Pardo-Casas & Molnar, 1987; Silver *et al.*, 1998).

TECTONIC HISTORY OF THE HUANCABAMBA ANDES

The sector of the Andes inland of the Talara area, known as the Huancabamba Andes or the Cordillera Real, stretches between 3°S and 8°S in southern Ecuador and northern Peru, and represents the connection between the Northern and the Central Andes (Figs 1 and 2). A distinguishing feature here is the directional variation in the Andean trend known as the Huancabamba deflection (Mourier *et al.*, 1988), from N 20°W in the northern part of the Central Andes to N 20°E in the Northern Andes (Fig. 1). The Huancabamba deflection is a major tectonic lineament that separates two intrinsically different sectors of the main Andean Cordillera: the Palaeozoic metamorphic belts of the Cordillera Real intruded by Mesozoic(?) plutons and the Peruvian Western Cordillera (Cordillera Occidental, Fig. 1) composed of Mesozoic sediments intruded by a Mesozoic arc (the Coastal batholiths) with younger Tertiary volcanics (Chew *et al.*, 2007).

Early Senonian onset of contractional deformation and calc-alkaline arc activity in the Huancabamban Andes is interpreted as the initiation of Farallon-Nazca plate

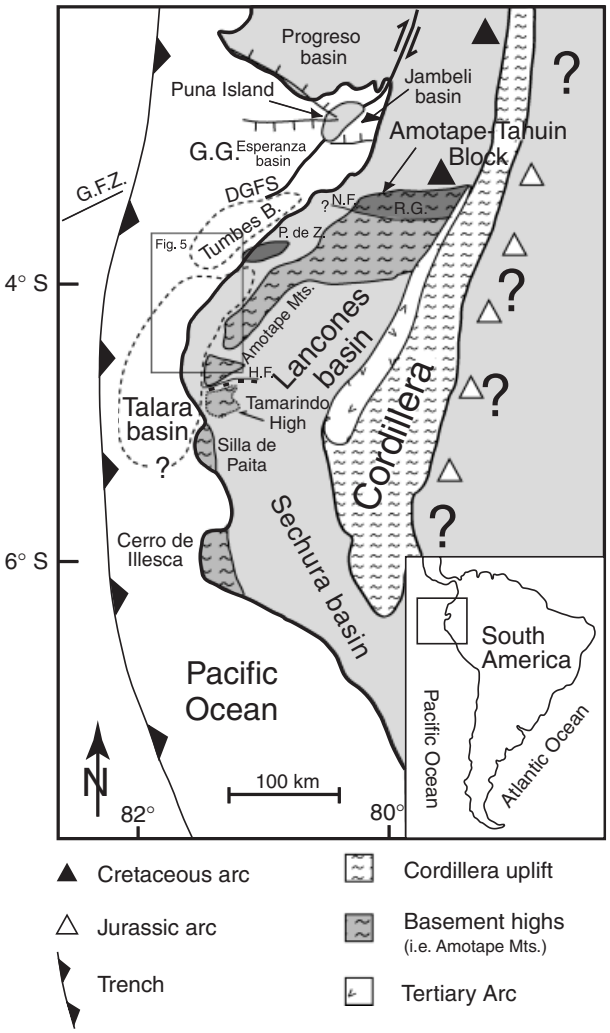

Fig. 2. Sketch map of the NW Peru Cordillera Real and location of major basins and tectonic lineaments. Talara and Tumbes basins extent highlighted with dashed lines. N.F., Naranjo Fault; R.G., Raspas Group; G.G., Gulf of Guayaquil; P.deZ., Pillars de Zorritos; H.F., Huayapira Fault; DGFS, Dolores–Guayaquil Fault System (map modified from Mourier *et al.*, 1988; Jaillard *et al.*, 1999; Fildani *et al.*, 2005; Spikings *et al.*, 2005; Witt *et al.*, 2006; Bourgois *et al.*, 2007).

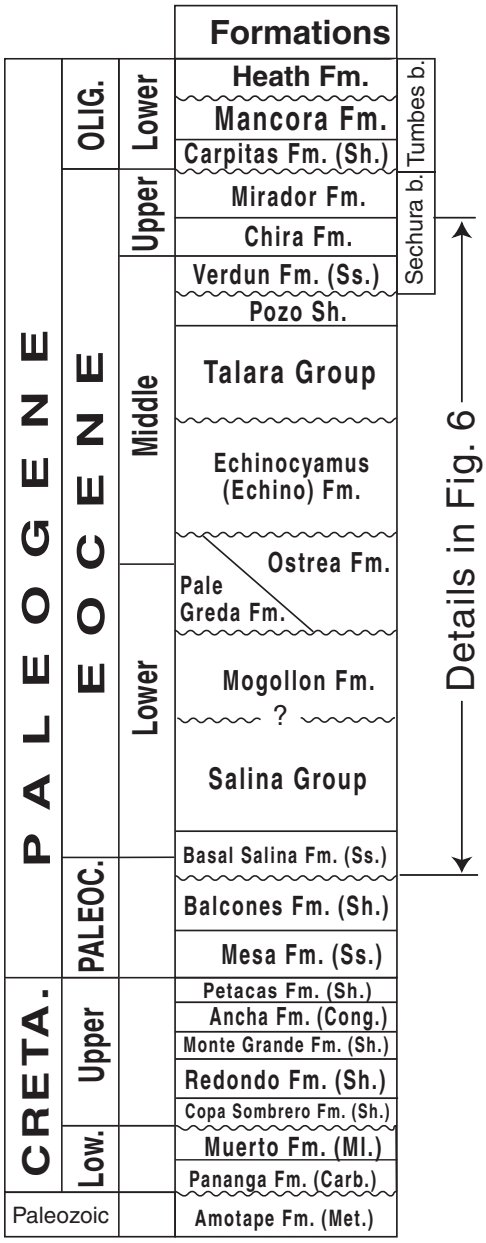

Fig. 3. Simplified stratigraphic column of Talara basin. This study focused on the Eocene section (modified from Marsaglia & Carozzi, 1991). Formations present in Sechura and/or Tumbes basins are noted to the right. Sh., Shale; SS., Sandstone; Cong., Conglomerate; Ml., Marls; Met., Metamorphic.

subduction (Benavides-Caceres, 1999) following westward drift of the South American plate as a consequence of the South Atlantic Ocean opening since the Albian (Nurnberg & Muller, 1991). Changing tectonic styles along the Andean margin since the Senonian are defined by major tectonic phases with not well-defined timing (Fig. 4). In the Peruvian Andes these tectonic phases have been linked to: (1) changes in convergence rates between the overriding South American plate and the Farallon-Nazca plate (Jaillard *et al.*, 1995), (2) successive clockwise rotations in the direction of convergence (Pardo-Casas & Molnar, 1987; Mayes *et al.*, 1990) and/or (3) absolute plate motion (Silver *et al.*, 1998). It is arguable that tectonic phases may span only a few million years per event, and perhaps these phases are better described by a continuum of convergence interrupted by periods of acceleration (Noblet *et al.*, 1996).

Presently, flat slab subduction and a volcanic gap are reported in the Andean portion inboard of the Talara basin (Bernal *et al.*, 2002; Lamb & Davis, 2003).

TECTONIC SETTING AND GEOLOGY OF TALARA BASIN

The Talara basin sits immediately eastward of the Nazca-South American plate boundary (Fig. 2). To the north, the

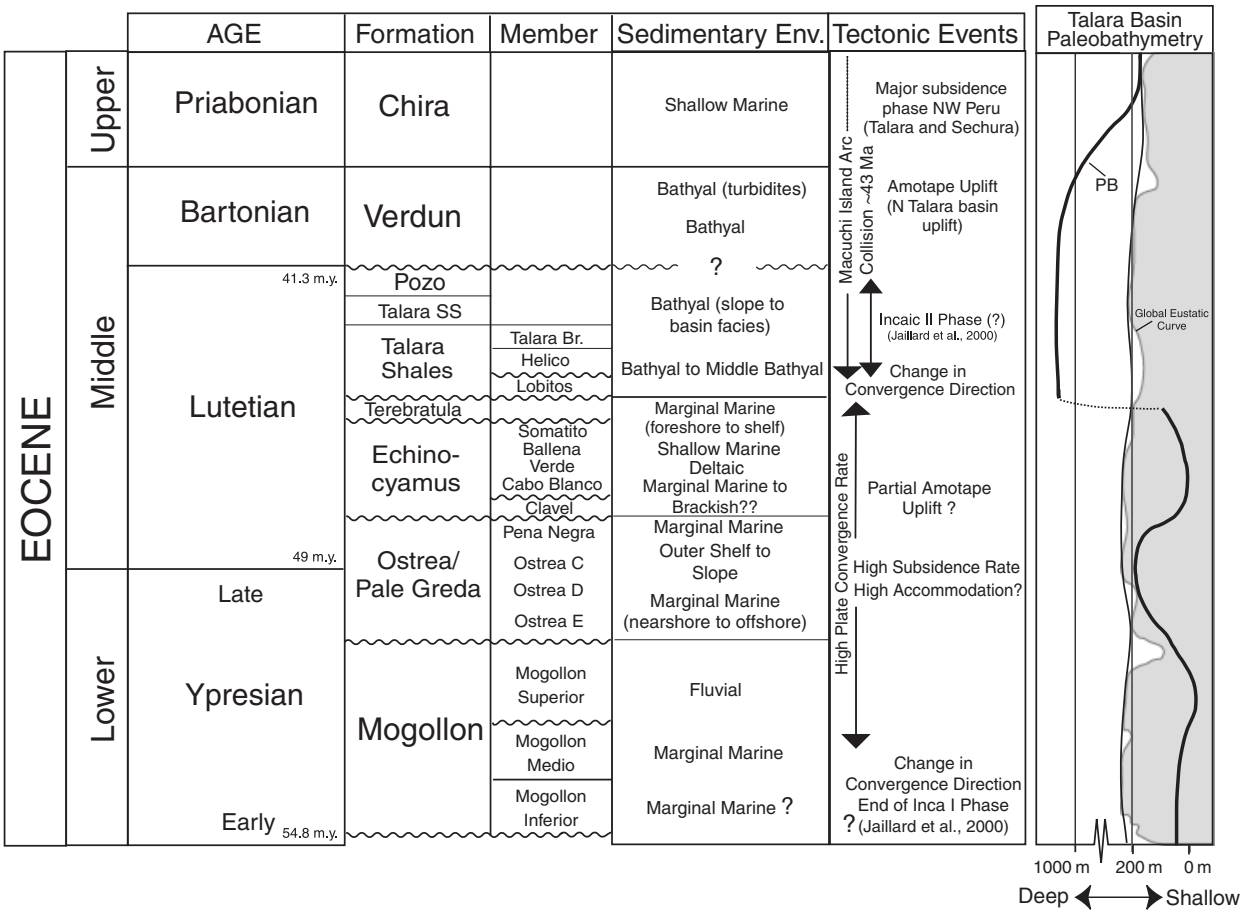

Fig. 4. Detailed stratigraphic section for Eocene strata of Talara basin with sedimentary environment interpretation for members and formations (this study) and their relation with major tectonic events (from this study, Benavides-Caceres, 1999; Jaillard *et al.*, 2000; Spikings *et al.*, 2005). Chronostratigraphy is based on data from Table 1 (based on Berggren *et al.*, 1995). The reconstructed palaeobathymetric curve (PB on Fig. 4, data reported on Table 1) is superimposed over the global eustatic sea-level curve (in grey) for comparison (sea-level curve from Hardenbol *et al.*, 1998).

Peru-Ecuador trench is dissected by a major tectonic lineament trending SW–NE that continues inland as the Dolores–Guayaquil Fault System (DGFS in Fig. 2). The DGFS represents a fundamental break in crustal structure along the South American margin (Shepherd & Moberly, 1981). The basement of western Ecuador, west of the fault system, may be an accreted fragment of an overthickened and buoyant oceanic plateau of Upper Cretaceous to Lower Palaeocene age (Reynaud *et al.*, 1999), whereas the basement south and east of the fault system has continental affinities (Shepherd & Moberly, 1981; Spikings *et al.*, 2005; Witt *et al.*, 2006). The Talara basin mostly overlies this 'continental-type' crust based on gravimetric studies (Lonsdale, 1978).

The DGFS delineates the southern end of the North Andean Block whose northward movement and subsequent extensional strain is the likely cause of detachment faulting and subsidence in the Gulf of Guayaquil (Fig. 2; Witt *et al.*, 2006). Recent (< 12 Myr) collision of the Carnegie Ridge with the trench caused interplate coupling, northward movement of the North Andean Block, and escape tectonics in the Gulf of Guayaquil in the last 2 Myr (Witt *et al.*, 2006). This has given rise to a tectonic mosaic of at least four different detachment-bound basins in the Gulf of Guayaquil: Progreso, Jambeli, Esperanza and Tumbes. (Witt *et al.*, 2006; Fig. 2).

Nowadays, the Lancones basin is separated from the Talara basin to the east by the Amotape Mountains, a topographic expression of the much larger metamorphic Amotape–Tahuin block (Fig. 2; Mourier *et al.*, 1988; Spikings *et al.*, 2005). The Tamarindo High is presently covered by sediments and it is the southern continuation of the Amotape–Tahuin block and part of a larger block together with the Silla de Paita and the Cerro de Illescas (Fig. 2), which currently isolates the Talara basin from the Sechura basin to the south. To the north, the Talara basin appears to be separated from the Tumbes basin by the 'Pillars de Zorritos', a series of enigmatic granitic intrusions encountered in drilling (Bush *et al.*, 1994). The present-day offshore western and southwestern margins remain conjectural. Active detachment faults and active subduction erosion for this margin suggest that the Talara basin could have been partially destroyed to the west (Bourgois *et al.*, 2007).

However, the Talara basin was not always isolated from these nearby basins. Intermittent activity along the Huaypira and other normal faults in the southern Amotape–Tahuin

block (Fig. 2) may have controlled interactions between the Talara, Lancones, and Sechura basins (Fildani, 2004). The Lancones basin is filled with Cretaceous sedimentary rocks unconformably overlain by upper Eocene strata described as coeval with the Verdun and Chira Formations of the Talara region (Valencia & Uyen, 2002), confirming a connection between the two basins during the late Eocene. The Verdun and Chira formations of the Talara basin extend into the Sechura basin (Fig. 3), but the late Oligocene to Miocene sequences of the Sechura basin do not extend to the Talara basin (Caldas *et al.*, 1980), suggesting complete separation of these two basins by the late Oligocene. North of the Talara basin, the Tumbes basin contains a thick accumulation of Oligocene and Miocene strata exposed along the southern edge of the Gulf of Guayaquil (Fig. 2). The Oligocene Mancora Formation filled a depocentre that straddled the Tumbes and Talara basins. The Progreso Basin, an extensional or pull-apart basin related to activity along the DGFS (Fig. 2), was contiguous to the Tumbes basin in the Miocene, but did not likely interact with the Talara basin at any point in its history.

Upper Oligocene and Miocene rocks are missing across most of the central and southern Talara basin, where Pliocene strata rest unconformably on Eocene strata.

METHODS

The present investigation uses data derived from outcrop-based sedimentary facies and biofacies analyses to build a palaeobathymetric history of the basin; sandstone composition data from modal petrologic analyses; conglomerate composition data from clast counts and inorganic geochemical analyses of shale and single clasts from conglomerate.

The stratigraphic framework presented here is one refined from Fildani (2004), Fildani *et al.* (2005), and Duerichen (2005). Foraminifera, nannoplankton, palynomorphs and macrofossils were used to constrain timing, palaeobathymetry, and palaeoenvironment of key stratigraphic levels in the basin (Fildani, 2004). Because of a lack of published palaeobathymetric zonations for the Palaeogene Peruvian sections, we used the California palaeobathymetric model of Ingle (1980) with modifications by Ingle *et al.* (1980). The data, summarized in Table 1, are included in appendix in Fildani (2004).

Modal composition for each of the 38 medium-grained sandstone samples was determined using the Gazzi-Dickinson point-counting method (Dickinson, 1970, 1985; Ingersoll *et al.*, 1984) (Table 2). More than 500-point counts were performed on each thin section by one operator (A. Fildani). Potassium feldspars were stained to facilitate their identification.

Forty shale samples from representative formations throughout the Eocene–Oligocene section, were analysed for major-, trace- and rare-earth elements (REE) with X-ray fluorescence spectrography (XRF) and inductively coupled plasma mass spectrometry (ICP-MS) at Washington State University GeoAnalytical Laboratories (Supplementary materials Tables S1 and S2). Conglomerate clast counts were performed on a regular outcrop 10×10 cm grid at eight locations (100 clasts per locations). Clast-count categories included: plutonic clasts (mainly granitoids), volcanic, white quartzite, black quartzite, sedimentary clasts (siltstone, shale and sandstone).

STRATIGRAPHY OF THE TALARA BASIN

The general stratigraphy of the Talara basin to date has developed out of both academic (Bosworth, 1922; Iddings & Olsson, 1928; Travis, 1953; Bellido, 1969; Gonzales, 1976; Marsaglia & Carozzi, 1991; Carozzi & Palomino, 1993; Fildani, 2004) and proprietary petroleum-related study. The oldest outcrops of the Tertiary deposits, the Lower Eocene Mogollon Formation, sit unconformably on pre-Cenozoic metasedimentary and granitoid rocks of the Amotape block. Upsection, there is fairly continuous marginal marine deposition of the Ostrea/Pale Greda, Echinocyamus, and Terebratula Formations, punctuated by minor unconformities and fluctuating (but shallow) water depths (Fig. 4). By the middle Eocene, a significant unconformity and marine flooding event separates the Terebratula from the Talara Formation, and the basin remains a deepwater depocentre through the middle Eocene Verdun Formation. These formations and unconformities are detailed in the following section.

Consensus on stratigraphic nomenclature and correlation in the Talara basin has been hindered by (1) structural partitioning due to horst and graben subsidence throughout the early Tertiary, (2) abrupt lateral facies changes due to the nature of marginal marine depositional systems and (3) the $\sim$20 000 km^2 blanket of Pliocene to Quaternary marine terraces or 'tablazos' (DeVries, 1988; Bourgois *et al.*, 2007) that obscure the Eocene section, except where incised by flash-flood quebradas (Fig. 5). Based on all available information, however, the Talara basin can be sub-divided into southern and northern palaeogeographic domains. Age control between the two domains is poor, but Seranne (1987) proposed a correlation between the northern and southern basin using a proprietary database, which has been modified using new data from Fildani (2004) (Fig. 6).

Palaeobathymetry for the Talara Basin was constructed from facies analysis combined with palaeontological (benthic foraminifera) and palaeoecological (ichnofossils and/or fossils) observations (Table 1; Fig. 4; Fildani, 2004). This palaeobathymetric curve strictly relates to the northern part of the basin where major deep-water sedimentation occurred and the majority of the data was collected, but it can tentatively be extended to the southern part of the basin.

DEPOSITIONAL ENVIRONMENTS AND PALAEO-DISPERSAL PATTERNS

The sedimentary fill of Talara basin consists of three major intervals, from bottom to top: (1) 4000–6000 m of

Table 1. Micropaleontological data for selected formations of Talara basin (microfauna description reported in Fildani (2004))

Formations	Benthonic foram		Calcareous nannoplankton		Palynology
	Environment	Age	Age	Zones (Okada & Bukry, 1980)	
Chira Fm. (outcrop)	Probable bathyal	Indeterminate	Barren		
Verdun (11/8-2)	Middle/low bathyal	Indeterminate	Barren		
Verdun (11/22-6)	Middle/low bathyal	Indeterminate	Barren		
Pozo (11/27-11)	Bathyal	Indeterminate	Indeterminate		
PZ1-11/6/01 (Pozo Sh.)	Bathyal (/)	Indeterminate	Barren		
Pozo (Well 3265)	Probable bathyal	Middle Eocene	Barren		
Talara ss. (11/16-3)	Marine	Indeterminate	Barren		
B. Talara (11/13-3)	Middle/low bathyal				
B. Talara (11/13-2)	Probable Bathyal	Indeterminate			
Talara Sh. (Monte- 11/27-2)	Middle/low bathyal	Indeterminate	Early middle Eocene	CP 10-13B	
Talara Sh. (11/20-6)	Bathyal				
Helico Mb. (TOO-H2)	Middle/low bathyal	Middle Eocene	Middle Eocene	Probable C14A	
Helico Mb. (TOO-H1)	Bathyal	Middle Eocene	Indeterminate		
Helico M. (TO1-H7 well AA80)	Middle Bathyal (?)	Middle Eocene	Indeterminate		
Helico Mb. @ P. La Cruz	Middle Bathyal (?)	Middle Eocene	Indeterminate		
Lobitos (11/23-4)	Middle/low bathyal	Indeterminate	Early middle Eocene	CP 10-13B	
Lobitos (11/17-5)	Middle/low bathyal	Indeterminate			
Lobitos (11/17-3)	Middle/low bathyal	Indeterminate			
Lobitos (Well 1768)	Bathyal	Middle Eocene	Middle Eocene	CP 12B-CP 13C	
Basal Talara (11/27-1)	Bathyal ?		Indeterminate		Non-Marine (Pinacee)
Top Echino @ Ter. (11/22-2)	Indeterminate	Indeterminate	Indeterminate		
Echino (11/27-6)	Outer Neritic	Indeterminate			
Clavel (11/29-1)	Marine (?)	Indeterminate	Indeterminate		
Clavel (11/27-4)	Marginal marine	Indeterminate			
Clavel (Well EA 9296)	Indeterminate	Indeterminate			Marginal marine (Eocene)
Clavel (outcrop)	Indeterminate	Indeterminate	Indeterminate		Probable Eocene-Oligocene
Pale Greda ? (11/15-1)	Probable Middle Bathyal		Late early Eocene	CP10-CP12A	
Ostrea II (Well AX 11)	Marginal marine	Indeterminate	Barren		
Ostrea (Well AA80)	Marignal marine	Indeterminate	Barren		
Mogollon Medio (Well 1944)	Indeterminate	Indeterminate	Barren		Marginal marine (Eocene)

Table 2. Raw point-count data for sandstone from the Talara basin, Peru

No.	Sample	Location	Qm	Qp	Cht.	Kspar	Plags	Lv	Lm	Ls	heav/ opaq	Detrital micas	Interstitial	Total Gr.
	Mogollon Fm.													
1	11/25-2	Well EA 1764	144	42	3	19	101	52	71	10	3	6	49	500
2	11/25-4	Well EA 1764	128	36	2	16	113	57	47	15	3	16	66	500
3	11/25-5	Well EA 1764	177	56	5	16	69	60	42	17	8	5	45	500
4	3/16-1	S 4 31′38.7″W81 4′55.7″	160	23	0	3	105	45	38	3	6	33	84	500
5	3/16-2	S 4 31′38.7″W81 4′55.7″	121	33	5	7	97	89	42	5	4	8	89	500
6	TM2-00	S 4 32′6″W81 4′41.2″	139	41	1	18	114	51	44	4	5	22	61	500
7	TM4-00	S 4 32′6″W81 4′41.2″	188	41	2	15	82	72	34	8	2	1	55	500
8	TM10-00	S 4 28′24.9″W 80 59′53.2″	174	47	0	7	92	62	25	8	10	11	64	500
9	TM12-00	S 4 32′28.6″W81 04′46.8″	128	19	1	13	101	61	32	3	11	32	90	500
	Helico M.													
1	T02HR1	Punta Restin	70	16	3	19	77	70	44	19	7	4	153+18	500
2	T01-PLC2	Punta Restin	102	17	9	34	83	77	25	9	5	10	122+7	500
3	T01-N2	S 4 28′47″W81 18′40″	98	20	10	28	73	124	30	14	5	8	85+5	500
4	T02PLON9B	Punta Lobitos North	99	29	4	23	73	113	23	16	3	3	110+4	500
5	T02Hrest1	Punta Restin	65	21	6	71	31	100	24	28	1	1	140+12	500
6	T01 92-4217	Punta Restin	95	23	9	29	69	150	53	13	1	4	51	500
7	T01 92-4123	Punta Restin	88	23	6	23	98	124	31	11	4	4	84+4	500
8	T01-PLC3	Punta La Cruz	75	29	5	22	71	93	32	10	5	9	133+16	500
	Verdun Fm.													
1	11/22-7	S04 32′55.0″W81 11′28.2′	227	19	5	13	91	13	24	7	4	8	89	500
2	11/24-1	S04 08′03.1″W80 58′05.6′	214	26	6	10	59	37	33	7	2	14	92	500
3	11/24-5	S04 10′30.2″W 80 54 57.1″	226	19	2	32	89	30	31	11	2	3	55	500
4	11/29-5	Well EA 8003	230	35	5	26	31	43	19	14	6	8	83	500
5	11/29-7	Well EA 8004	182	32	6	19	62	50	38	35	2	5	69	500
6	11/30-6	S04 10′56.6″W81 08′ 00.4″	210	32	7	24	46	25	36	12	0	11	97	500
7	3/16-3	Quebrada Parinas	215	9	2	16	53	31	34	23	22	50	61	500
8	3/20-3	Taime Field	225	40	5	8	64	18	19	12		16	101	500
	Echino Fm.													
1	11/17-1	S04 25′22.0″W81 15′53.1″	137	27	0	29	72	35	42	7	10	27	114	500
	Terebratula Fm.													
1	11/18-1	S 04 25′36.1″W81 15′52.3″	152	3	2	37	128	37	29	1	3	4	104	500
2	11/18-3a	S 04 25′36.1″W81 15′52.3″	124	20	1	24	70	67	59	3	1	16	115	500
3	11/18-3b	S 04 25′36.1″W81 15′52.3″	111	15	1	29	85	67	39	4	1	16	132	500
4	11/22-3	S 04 25′37.0″W81 15′51.4″	138	8	7	28	86	40	36	2	0	10	145	500
	Ostrea Fm.													
1	4/11-01	S 4 16′25″W81 15′9.6″	168	28	3	18	79	78	32	2	6	9	77	500
2	T01-00	S 4 16′25″W81 15′9.6″	182	25	5	20	58	57	45	14	4	12	78	500
3	3/20-1	S 4 16′25″W81 15′9.6″	162	31	2	17	68	55	36	10	1	7	111	500
	Pale Greda Fm.													
1	11/11-2	S 04 31′24.8″W81 05′32.5″	183	21	2	6	83	27	39	1	2	31	105	500
2	11/10-3	S 04 31′34.5″W81 04′58.8″	212	27	2	5	97	25	20	1	1	5	104	500
	Cabo Blanco M.													
1	TCB1-00	S 04 13′40.6 W 81 12′13.1″	310	24	5	18	20	13	50	0	0	1	59	500
2	TCB3-00	S 04 13′39.2 W 81 12′07.2″	313	36	3	21	7	16	45	5	0	6	48	500
3	11/21-3	S 04 13′39.2 W 81 12′07.2″	374	29	2	3	12	13	36	1	0	2	28	500

Counted parameters.
Qm, Quartz monocrystalline; Qp, Quartz polycrystalline; Cht, Chert; Kspar, Potassium feldspar; Plags, Plagioclase feldspar; Lv, Volcanic lithic; Lm, Metamorphic lithic; Ls, Sedimentary lithic; Heav, Heavy minerals; cmt, cement; mat, matrix.

Palaeocene to middle Eocene shallow-marine mudstone punctuated by fluvio-deltaic to shallow-marine coarse siliciclastic sediments, (2) 1500–3000 m of middle to late Eocene deep-water turbiditic sandstone and conglomerate units within fine-grained sandstone and mudstone background and (3) 1500 m of latest Eocene to Oligocene shallow-marine siliciclastic sediments (Marsaglia & Carozzi, 1991; Carozzi & Palomino, 1993; Fildani, 2004; Duerichen, 2005). This study focuses on outcrop data from the earliest two intervals.

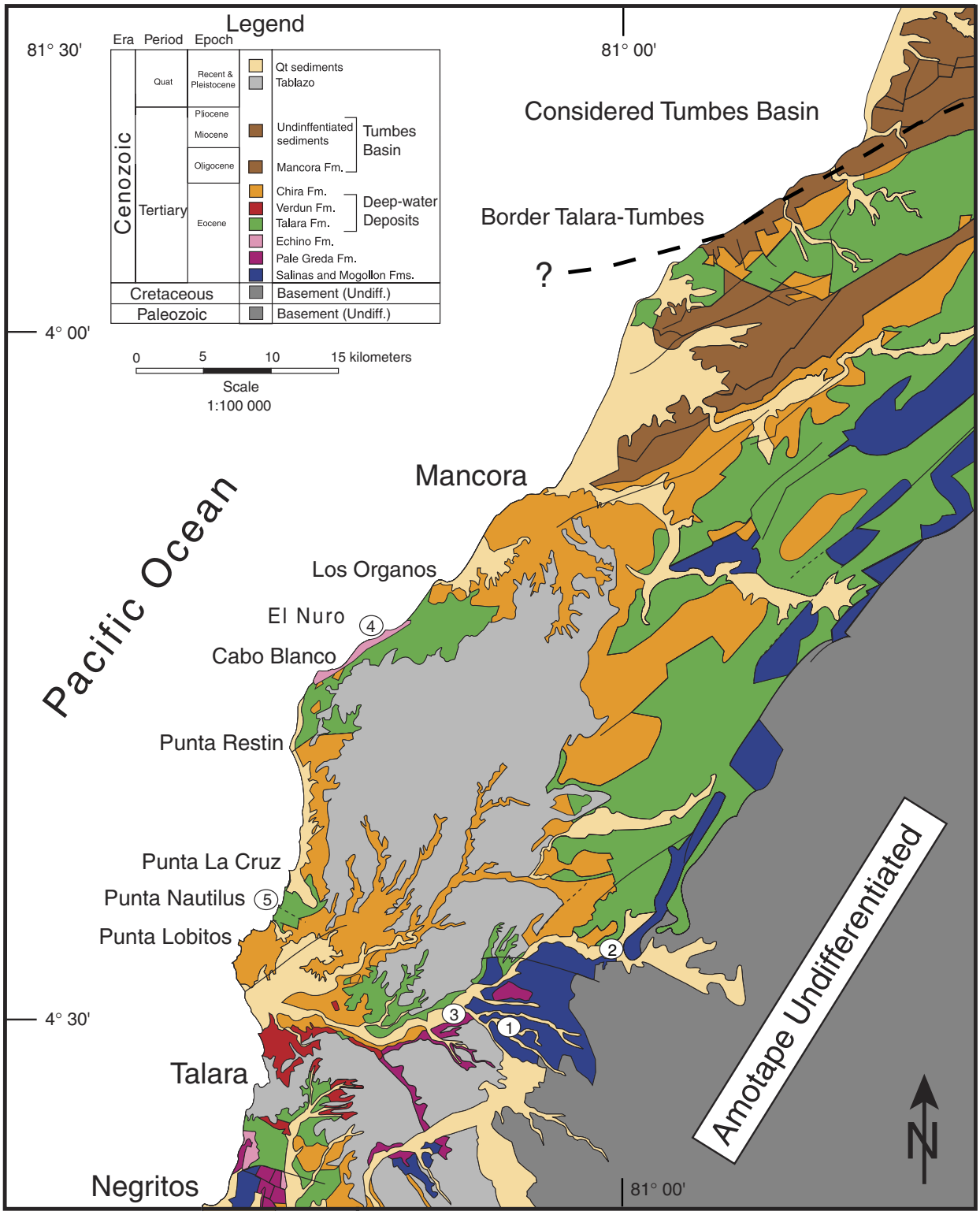

Fig. 5. Geologic map of the Peru coastal area (scale 1 : 100 000 – modified and simplified from Bellido, 1969 and INGEMMET, 1999). Only the Eocene interval is discussed in details in this paper. (1) Location of measured section on Fig. 7a; (2) Location for sketched measured section from Quebrada Angostura on Fig. 7b; (3) Reported Pale Greda section in Fig. 7c; (4) Cabo Blanco Member outcrops characterized in Fig. 9a; (5) location of measured section of Terebratula Fm. in Fig. 9b.

Mogollon and Pale Greda formations

The lower Eocene Mogollon Formation is the oldest formation to crop out continuously in the eastern portion of the Talara basin with a maximum thickness of ~700 m (Fig. 5). It is interpreted as a braided fluvial deposit based on thick cross-bedded sandstone, conglomerate and the occurrence of large flow-parallel tree trunks

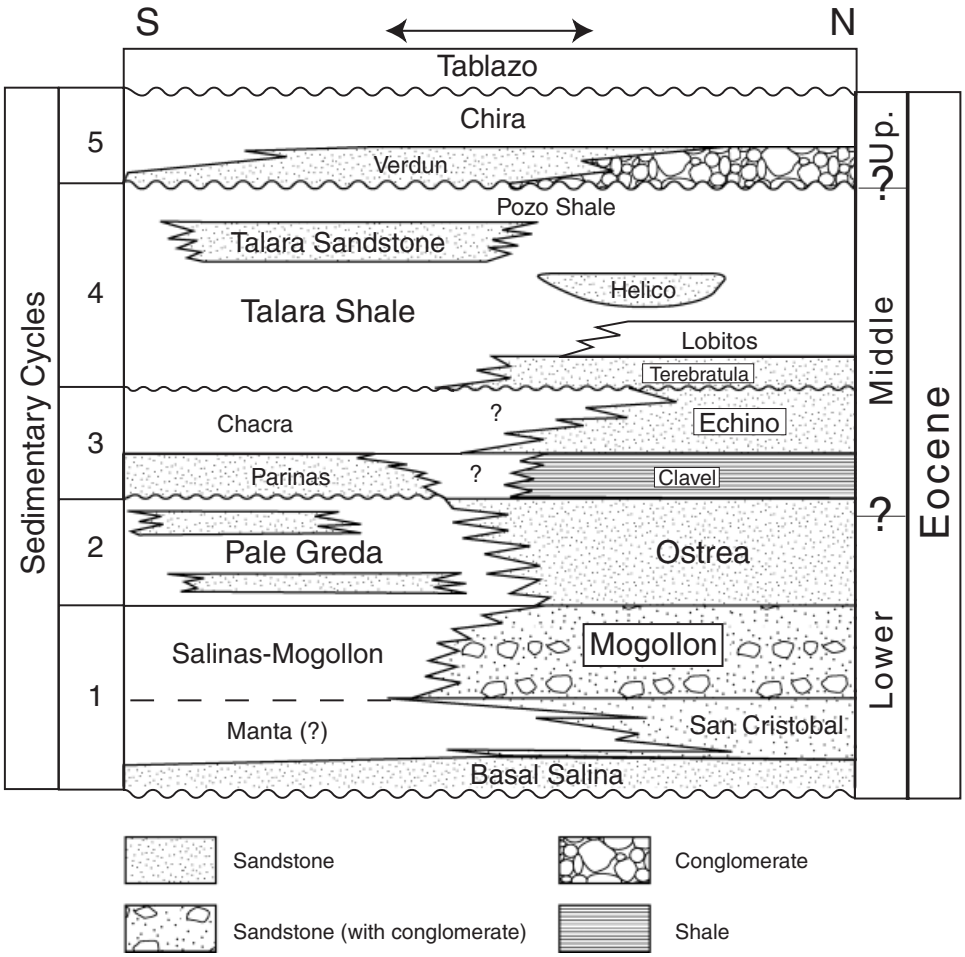

Fig. 6. Correlation between northern and southern depositional areas and main sedimentary cycles of Talara basin (Modified after Seranne, 1987; unpublished data PetroPeru).

(Figs 7a, b and 8) (Fildani, 2004). Palaeocurrent data from clast imbrication and cross-sets clearly indicate a predominant west and northwestward palaeo-flow direction (Figs 7a, b and 8a–d). From unpublished subsurface data (courtesy of Perez Companc) the Mogollon Formation is correlatable to shallow marine facies to the west and south. Together, these relations define an NE–SW transition from non-marine to marine facies (Fig. 6).

The uppermost Mogollon Formation, composed of medium- to fine-grained sandstone with faint planar laminations, may represent the gradual transition from fluvial to marginal marine deposition of the overlying Pale Greda Formation. The contact between the Mogollon and Pale Greda Formations is marked by the first appearance of unequivocal marine deposition: a thick shell fragment-rich bed (mostly gastropods and oysters) interpreted as coquina bed (Figs 7c and 8e). The Pale Greda Formation is composed of marine shale and siltstone with intercalated sandstone and common coquina beds, which contain progressively fewer gastropods and more oyster shells upsection. Because of its sedimentary packaging and biofacies associations (Weiss, 1955; Fildani, 2004), this formation has been interpreted as a shallow-marine deposit that deepens upsection (Fig. 7c) (Fildani, 2004). The equivalent of the Pale Greda Formation to the north is the Ostrea Formation (Fig. 6), which crops out very sparsely but has been studied in core and logs in the subsurface (Perez Companc, now Petrobras S.A., proprietary data). Both the Ostrea and Pale Greda Formations are characterized by shallow-marine shelf elements; however, the more sand-rich Ostrea Formation was likely deposited closer to a source of coarse detrital material (Fildani, 2004). The Ostrea Formation reaches a maximum thickness of ~1100 m (Picarelli *et al.*, 2003). Transition to the unconformably overlying *Echinocyamus* Formation is only observed in the subsurface (Fig. 11) (Fildani, 2004).

The *Echinocyamus* formation

The *Echinocyamus* Formation (hereafter shortened to Echino) is composed of five members: Clavel, Cabo Blanco, Verde, Ballena and Somatito for an overall thickness of ~400 m (Daudt *et al.*, 2004). The Clavel and Cabo Blanco members are the only Echino Formation members to crop out, other than a few metres of the Somatito Member accessible in a limited outcrop along the coast. The Clavel Member is a green–grey shale barren of microfossils (Fildani, 2004; see Table 1). The top few metres of the Clavel Member are pervasively bioturbated, overlain by shell lags and metre-scale cross-bedded, quartz-rich sandstone of

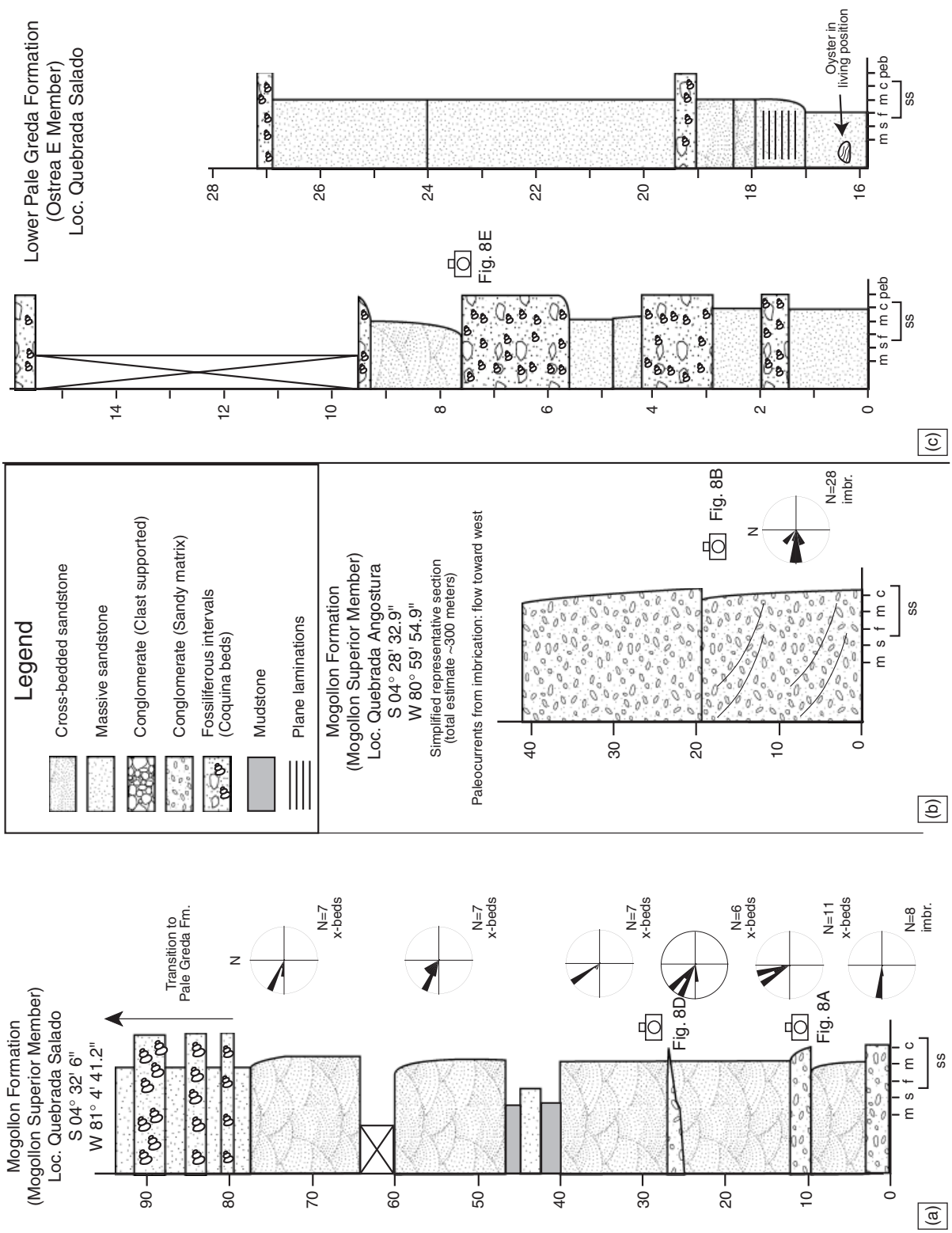

Fig. 7. (a) Simplified measured section of the Upper Mogollon Formation in the Quebrada Salado with transition to Pale Greda Formation and (b) simplified measured section from Quebrada Angostura. (c) Measured section of the lower Pale Greda Fm. in the Quebrada Salado (Locations on Fig. 5). Rose diagrams indicate persistent NW directed palaeoflows. Thickness in metres.

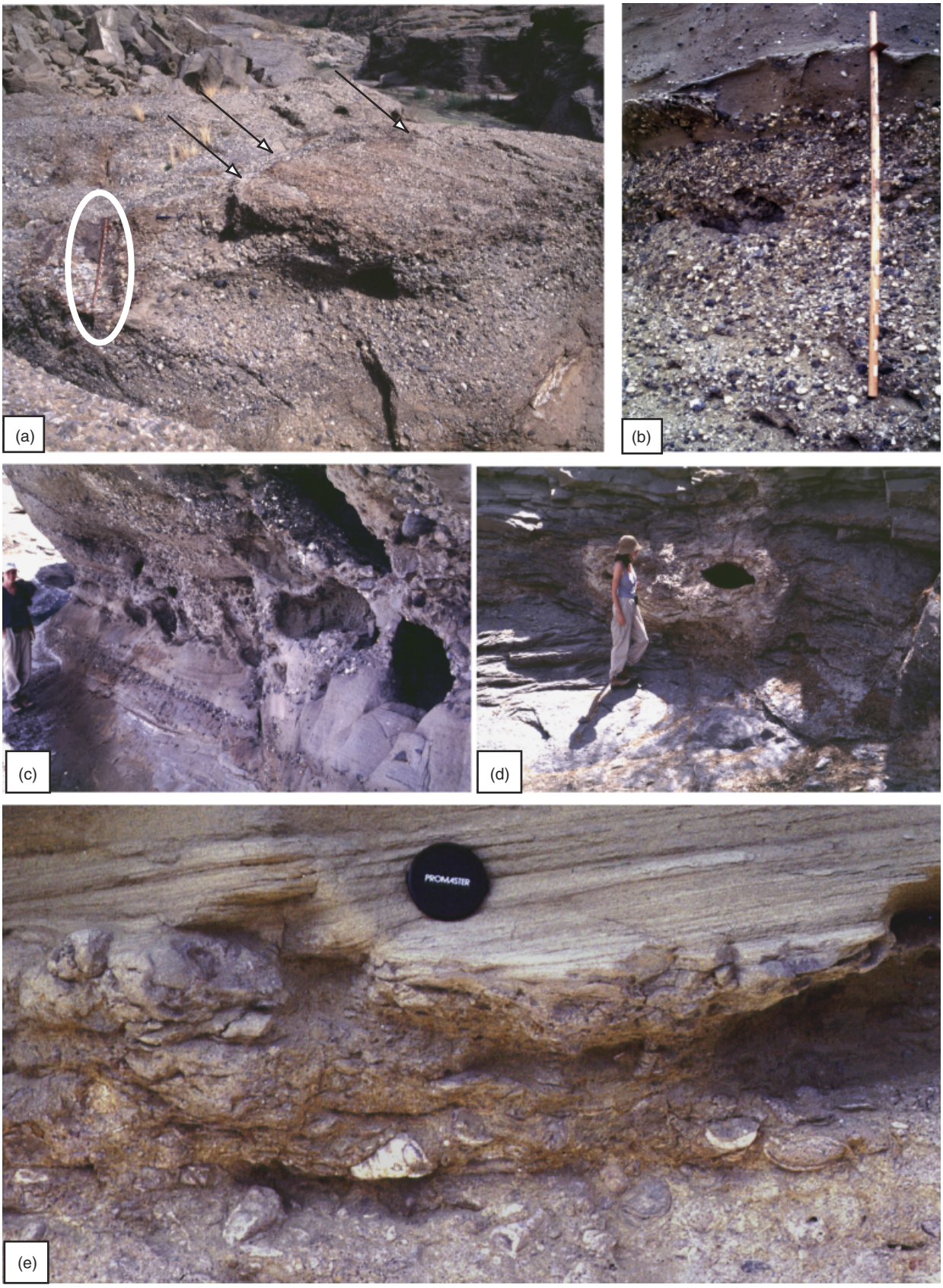

Fig. 8. Mogollon Formation typical outcrops. (a) Faint cross-beds in pebble conglomerate (arrows indicating beds, 1.5 m Jacob's staff for scale). (b) Pebble-conglomerate in sandy matrix. (c) Large (40–50 cm) rip-up mud clasts in cobble-conglomerate with sandy matrix. (d) Large cavity left by a tree-trunk in cross-bedded sandstone. (e) Coquina beds of the Pale Greda Formation overlain by cross-stratified sandstone.

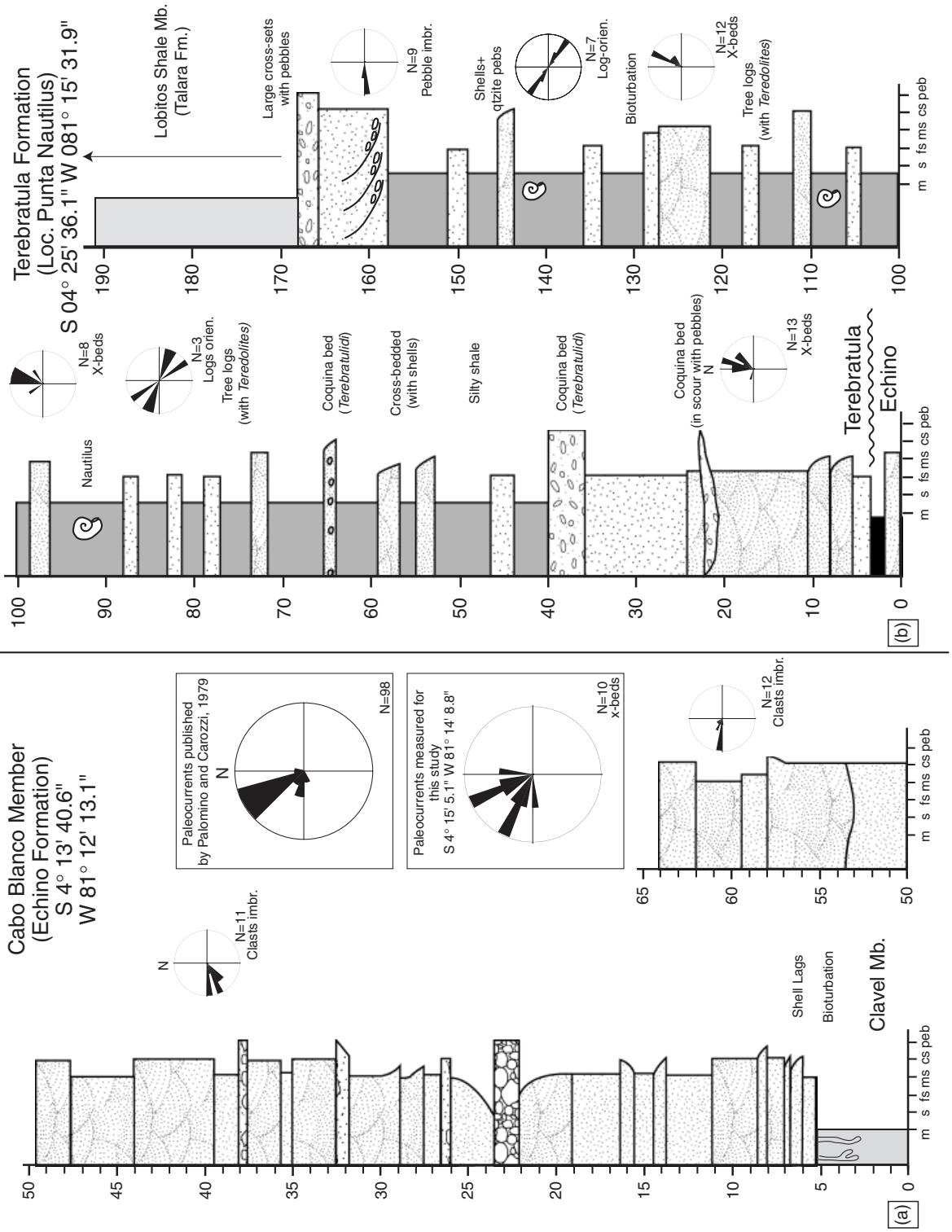

Fig. 9. (a) Simplified measured section of the Cabo Blanco Member sandstone in coastal outcrops of El Ñuro. Rose diagrams indicate west directed palaeoflows. (b) Detailed measured section of the Terebratula Formation with transitions from the Echino Fm. (bottom) and Lobitos Shale (top) (Locations on Fig. 5). Thickness in metres.

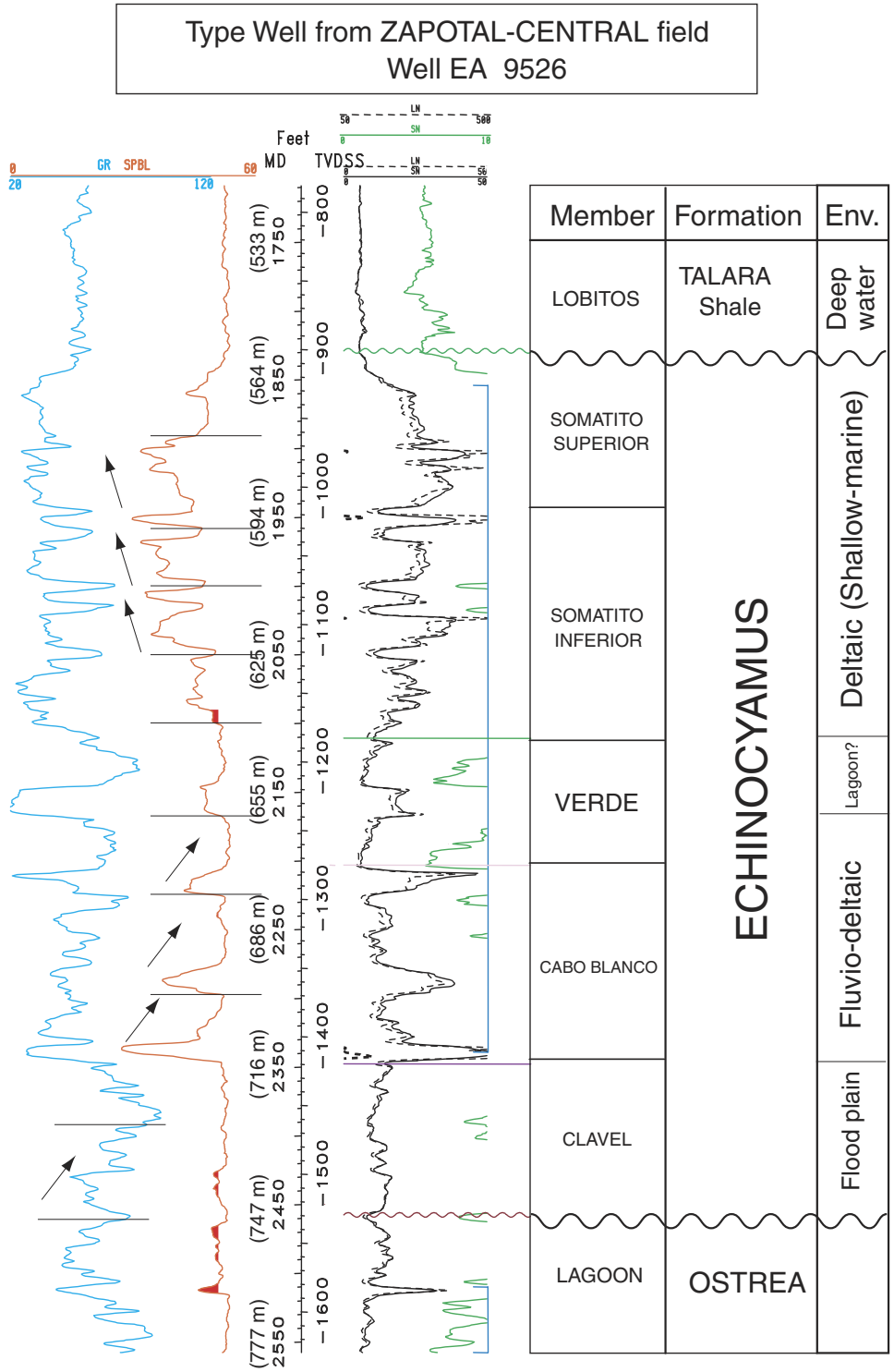

Fig. 10. Resistivity and γ-ray well log record from the northern portion of the basin (Block X), showing the typical stacking pattern of the Echino Formation (courtesy of Perez Companc del Peru). Env., Interpreted depositional environment.

the lower Cabo Blanco member (Fig. 9a). Upsection the Cabo Blanco member contains lenticular sandstone beds, fine-sandstone beds with oyster bioherms, *Turritellae* shell lags and bioturbated siltstone are present; inferred sediment dispersal is westward (Fig. 9a). The Cabo Blanco Member has been interpreted as a mixture of fluvial and deltaic conglomeratic sandstone deposited from east to west (Palomino and Carozzi, 1979; Daudt *et al.*, 2004; Fildani, 2004). Combined outcrop and proprietary subsurface data for the Echino Formation support the interpretation of the five members as successive fluvio-deltaic to deltaic and/or shallow marine deposits stacked in a prograding fashion (Fig. 10) (cf. Van Wagoner *et al.*, 1990). This interpretation is in agreement with the Daudt *et al.* (2004) interpretation of the Echino being a 'regressive megacycle'.

The Talara Group: Terebratula and Talara Formations

A major basin-wide depositional transition occurs between the Echino, Terebratula, and Talara Formations. The Terebratula Formation (~200 m) overlies the cross-bedded sandstone of the Somatito Member (Echino Formation) in apparent angular discordance (Fildani, 2004). Gutierrez & Arriola (2002) indicated a ~2 m.y. hiatus between the Echino Formation and Terebratula Formation using well data. The Terebratula Formation is characterized by 2- to 3-m-thick cross-bedded sandstone beds with pebble- and shell-filled scoured bases. Conglomerate beds are also present. Coquina beds contain common brachiopods (*terebratulidi*) and *Turritellae*. Upsection, pervasively bioturbated shaly siltstone becomes predominant with interbedded cross-bedded thin layers of pebbly sandstone and shells (Fig. 9b). This formation is interpreted to reflect progressive deepening from foreshore to outer shelf depositional environments (Fildani, 2004).

The overlying Talara Formation represents the first deep-marine deposits in the Talara basin (Fig. 4) with a maximum thickness of ~700 m (Picarelli *et al.*, 2003). The shaly Lobitos Member (~80 m), deposited in a deep-water environment on the palaeoslope of the basin (see palaeobathymetric reconstruction from Table 1), unconformably overlies the shallow marine Terebratula Formation. Based on benthic foraminifera (Table 1; details reported in Appendix for Fildani, 2004), deepening of the basin appears to have been rapid, with water depth changing from < 200 m during deposition of the Terebratula Formation to upper bathyal depths of the Lobitos Member and middle bathyal of the overlying Helico Member.

Interbedded shale and pebbly sandstone deposits of the Helico Member (~300 m) are re-sedimented gravity flows (*sensu* Bouma, 1962; Lowe, 1982) and show palaeocurrent patterns indicating a northwestward trend very similar to that of the Mogollon Formation (Fig. 11b). However, the overlying deepwater turbidite of the Talara Sandstone Formation, which outcrops as discontinuous sandstone beds within the background shale of the Talara Formation (Fildani, 2004), indicate a WSW palaeoflow direction (Fig. 11c; Fildani, 2004; Duerichen, 2005).

Eventually, the Pozo shale blanketed the entire basin to end the first stage of basin-wide deep-water deposition. Biofacies assemblages confirm a widespread deep-water environment across Talara during Pozo time (Gutierrez & Arriola, 2002) and are supported by this study (Table 1).

Verdun and Chira formations

The second and final deep-water episode in the Talara basin deposited the Verdun-Chira formations immediately following the Talara Group. Gutierrez & Arriola (2002) proposed a hiatus of ~1 m.y. between the Talara Group and the Verdun Formation. The Verdun Formation varies in thickness, from about 400 to 620 m, and was deposited basin-wide (Duerichen, 2005). It is composed of thick conglomerate and sandstone intervals interbedded with thin-bedded sandstone and mudstone and it is interpreted as a turbidite system, where palaeocurrent data consistently indicate a southwestward palaeoflow (Fig. 11d). This palaeodispersal pattern differs significantly from that observed in underlying formations (Fig. 11). Using nannoplankton data, Duerichen (2005) attributed the Verdun Formation to the late Eocene. The Verdun Formation is overlain by the Chira Formation, a basin-wide marine mudstone (Carozzi & Palomino, 1993). Bio-facies associations indicate that uppermost sediments of this formation were deposited in a shallow marine environment (Fildani, 2004; see Table 1).

PROVENANCE ANALYSIS

Conglomerate clast composition

Throughout the Talara basin, conglomerate units consist of mature, well-rounded pebbles of highly resistant rock types like quartzite, chert, and low-grade metamorphic rock. However, variations between the major sedimentary units are observed in detailed clast counts (Fig. 12).

Mogollon Superior conglomerate units contain abundant quartzite, in addition to lesser felsic volcanic and granitoid clasts. Intermediate volcanic clasts of greenish colour (described by the local geologists as 'andesita') are present in both localities but were most easily identifiable in the Quebrada Angostura outcrop (Fig. 12).

Helico Member conglomerate units are rich in quartzite and contain volcanic clasts (sub-rounded to rounded intermediate volcanic clasts showing microlitic, porphyritic, lathwork, and vitric textures) and very few plutonic and recycled sandstone pebbles. Overall, the Helico Member conglomeratic units show a ~20% increase in volcanic clasts with a marked increase in intermediate varieties (Fig. 12).

Verdun Formation conglomeratic units contain easily recognizable sandstone intraclasts (fine-grained sandstone and shale matrix supported), microcrystalline chert, and granitic cobbles. Very few intermediate volcanic clasts were observed in outcrops but never occurred within analysis grids (Fig. 12).

Sandstone petrography

Previous petrographic studies in the Talara basin (Marsaglia & Carozzi, 1991; Carozzi & Palomino, 1993) have reached comparable conclusions: derivation from a fairly uniform mineralogical province producing quartz-rich sand with only minor volcanic input. However, only the Basal Salina Formation, a pre-Mogollon (Palaeocene) fan-delta deposit restricted to the subsurface, has been studied in detail (Marsaglia & Carozzi, 1991; Fig. 13d). Basal Salina sandstone plots within the recycled orogen, and the presence of plutonic and high-grade metamorphic

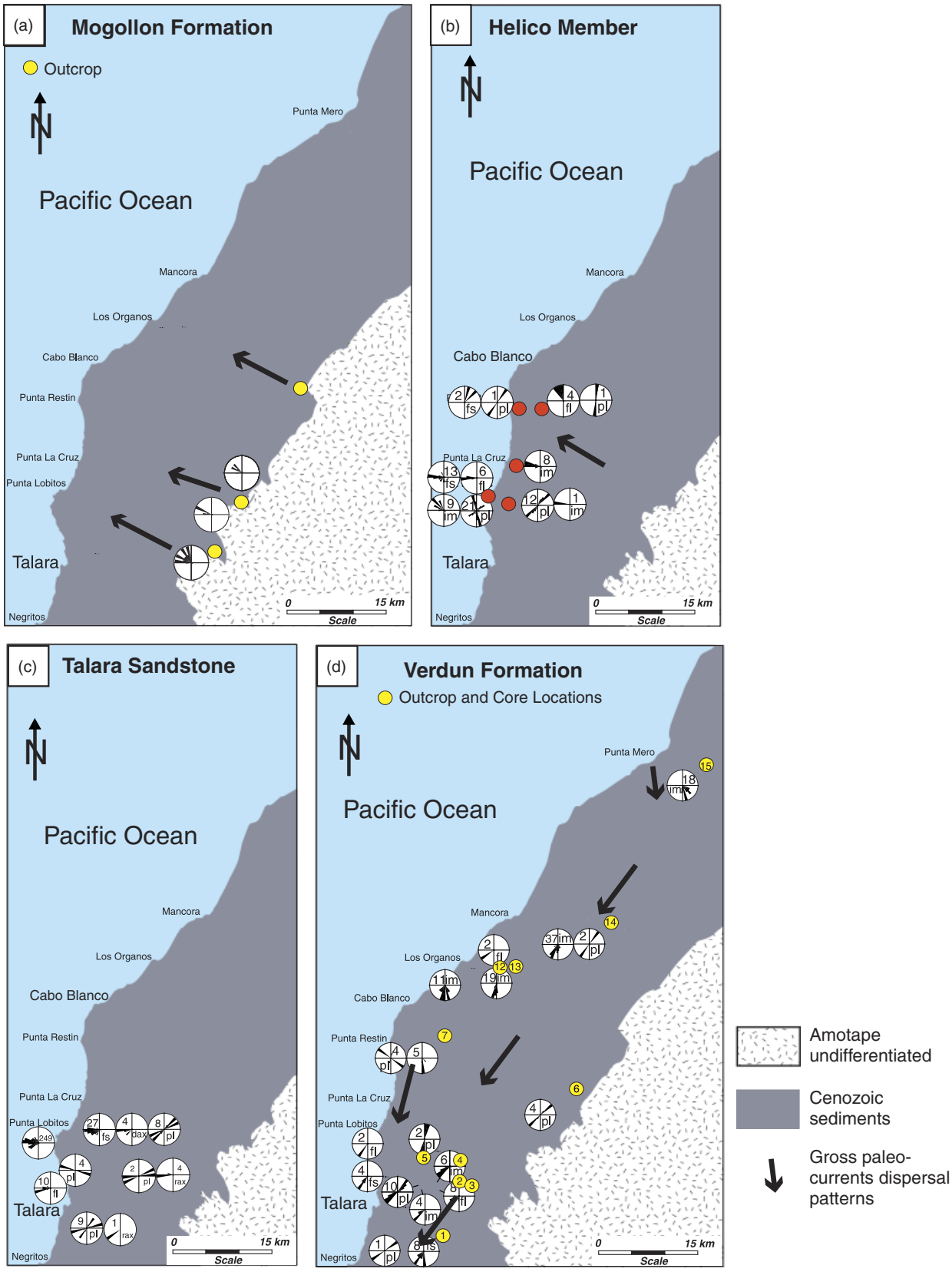

Fig. 11. Palaeocurrent distribution patterns for the Mogollon Formation (a), the Helico Member of the Talara Formation (b), Talara Formation (c), and Verdun Formation (d). Arrows indicate gross palaeo-dispersal trends. Figure modified from Duerichen (2005). Data for Talara Formation, Helico Member and Verdun Formation are from Duerichen (2005).

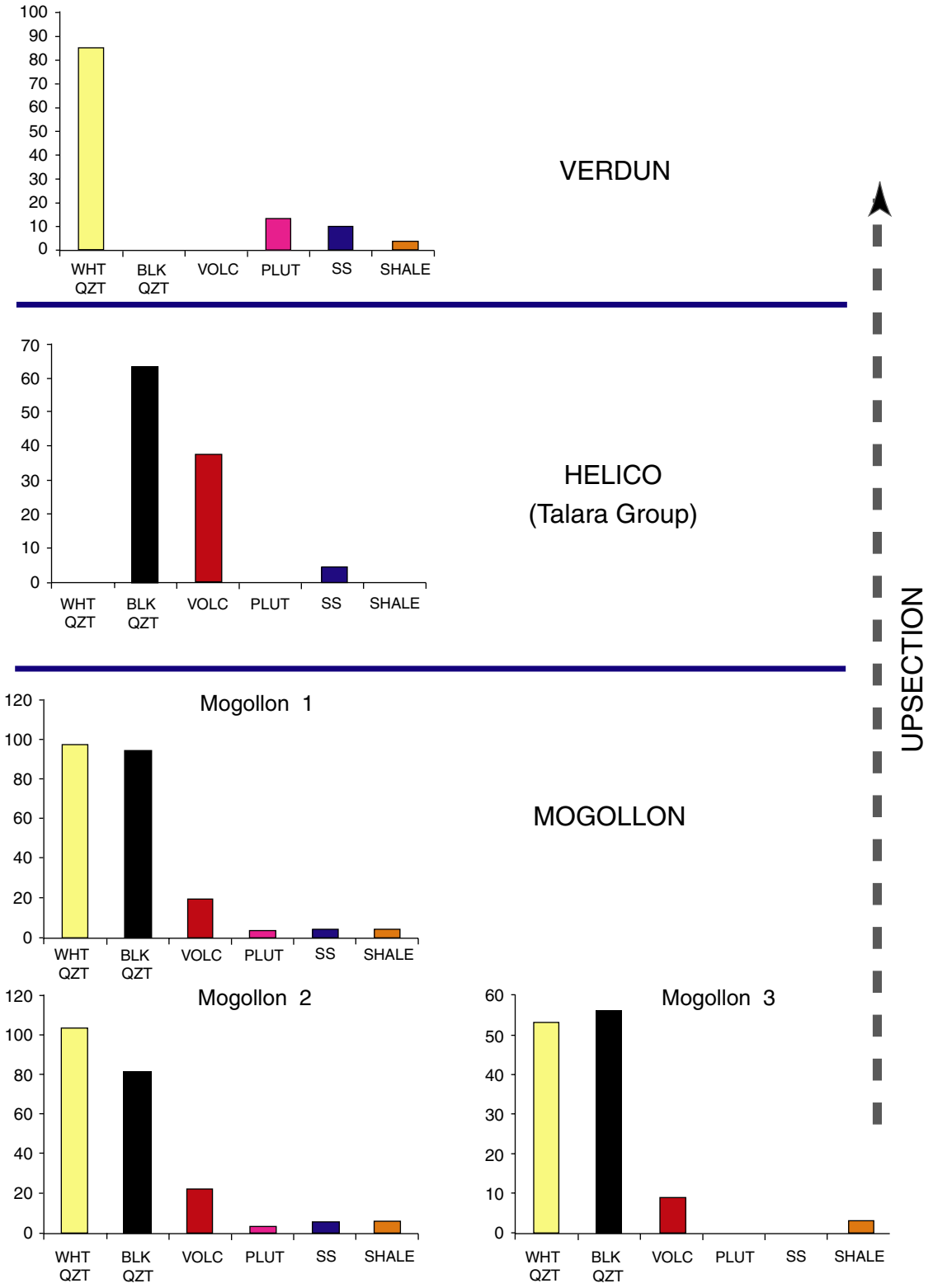

Fig. 12. Conglomerate clast counts results of major conglomeratic units of Talara basin. WHT QZT, white quartzite; BLK QTZ, black quartzite; VolC, volcanic rocks; PLUT, plutonic rocks; SS, sandstone; SHALE, shale. Data from Fildani (2004).

fragments is interpreted to reflect derivation from an ancient Amotape highland and its cover sequences (Marsaglia & Carozzi, 1991) (Fig. 13d).

Petrographic data are presented in Table 2, and sandstone detrital modes are summarized on ternary diagrams in Fig. 13.

Mogollon Formation arenites are weakly cemented by calcite and clay minerals. Quartz (angular to subangular) and feldspar are the dominant framework grains, with plagioclase more common than potassium feldspar (Fig. 13c). Quartz grains exhibit varying degrees of undulose extinction, and polycrystalline quartz grains are common. Mo-

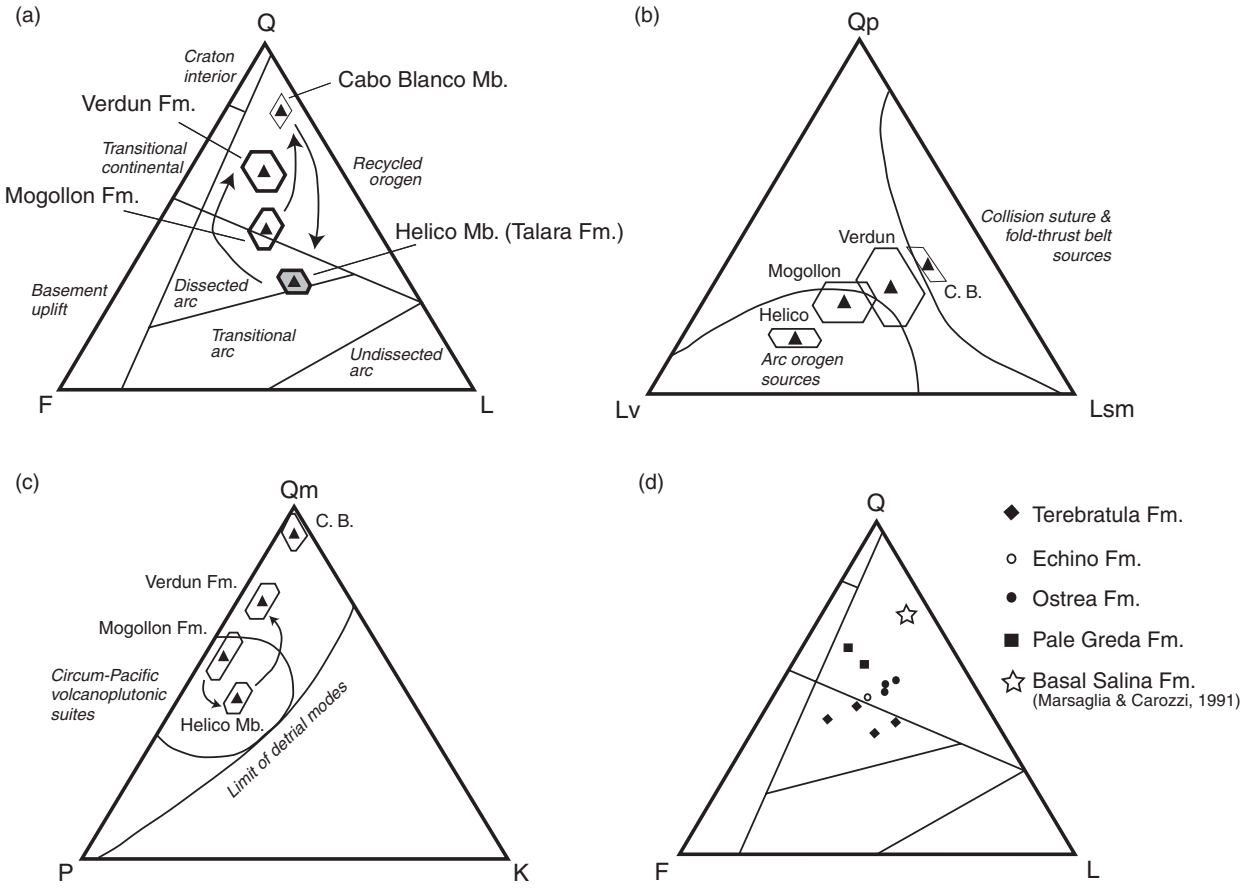

Fig. 13. Sandstone detrital mode normalized into grain categories for comparative petrography and displayed on ternary diagram with their mean values and their standard deviation; (a) quartz, feldspar and lithic components (QFL), (b) quartz policrystalline, lithic volcanic and lithic sedimentary + metamorphic (QpLvLsm), and (c) quartz monocrystalline, plagioclase and k-feldspar (QmPK) as the apexes. (d) QFL diagram displaying samples (not enough for statistical mean and standard deviation) from Terebratula, Echino, Ostrea, and Pale Greda fms compared to mean value for Basal Salina Fm. Compositional fields are from Dickinson (1985) (Table 2). Arrows indicate sequential stacking of formations from bottom (Mogollon Fm.) to top (Verdun Fm.). C.B., Cabo Blanco Member.

gollon Formation sandstones contain a diverse population of lithic volcanic and metamorphic grains. Volcanic grains range from angular to sub-rounded and are fine-grained, microlitic, and intermediate to basaltic in composition. Fine-grained quartz-rich volcanic lithic fragments and some tuffaceous grains are present. Metamorphic fragments include metaquartzite and schist (Table 2).

The Cabo Blanco Member sandstone is composed almost entirely of monocrystalline unstrained quartz. A few feldspars (mainly potassium-feldspar) and lithic metamorphic grains are present. Lithic volcanic grains are rare.

The Helico Member sandstone contains abundant lithic volcanic (vitric volcanic and microlitic intermediate with some lathwork grains) and only minor plutonic fragments and sedimentary lithics (siltstone and fine-grained sandstone). Metamorphic fragments are schistose (Table 2). Many of the volcanic grains in the Helico Member are significantly altered but still recognizable.

Quartz is the dominant constituent of the Verdun Formation sandstone (Fig. 13), mainly represented by unstrained angular quartz with minor undulose strained grains. Grains are sub-angular to sub-rounded with 10–15% open pore space area between grains and occasional traces of mud matrix. Some quartz grains are rounded to sub-rounded. Plutonic grains contain perthitic, microperthitic and myrmekitic intergrowths. Volcanic grains are present but not common. Metamorphic fragments include metasandstone (and siltstone) and schist. Rare fragments of siltstone and argillite are also present (Table 2).

The composition of the Talara Sandstone is similar to the sandstone of the Verdun Formation but slightly richer in volcanic lithic grains (Duerichen, 2005). The values reported by Duerichen (2005) are not included in statistical analyses here owing to differences in petrographic methods.

Shale geochemistry

REE geochemistry of shale was used to track components of the source area that might not be represented in the sand fraction. Of the sedimentary size fractions, shale is thought to give the best estimate of average provenance (Taylor & McLennan, 1985). Immobile elements (e.g. REE) are only slightly affected by geochemical and mineralogical changes during source-area weathering

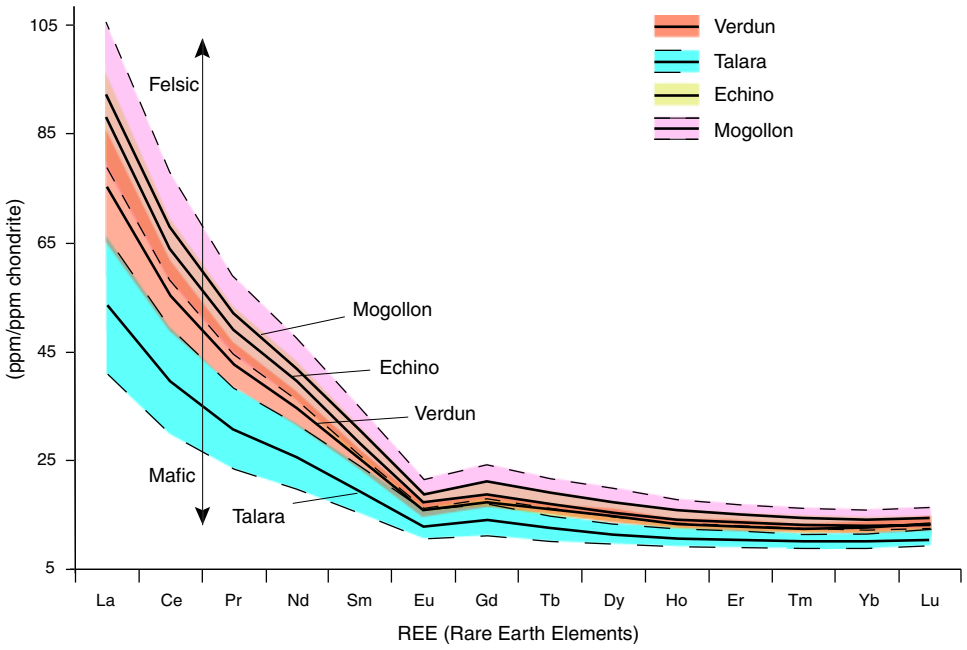

Fig. 14. Fractionation diagram for REE comparing major formations of Talara basin. Patterns are shown as average (dark-line), with one standard deviation (shaded colours) (Supplementary Tables S1 and S2). REE, rare-earth elements.

(McLennan, 1989; Cullers *et al.*, 1993; Hessler & Lowe, 2006). REE in shale are considered particularly reliable provenance tracers because of their relative insolubility during weathering and sedimentary transport (McLennan, 1989). We investigated REE abundance and fractionation assuming that a high mass-related REE fractionation corresponds to silt and clay weathered from felsic source rocks, whereas low mass-related REE fractionation implies a mafic source for silt and clay (Nesbitt, 1979).

On a plot of average, chondrite-normalized REE values (Fig. 14), the oldest shale (Mogollon Fm.) shows the highest degree of mass-fractionation, and therefore the most felsic composition of the basin shales. Upsection, the Echino shale has a slightly smaller mass-fractionation than the Mogollon shale, showing increased relative input of more mafic-derived clays. REE show intermediate mass fractionation for the overlying Talara group, making this shale the most mafic in the basin. The overlying Verdun shale shows a significant increase in felsic material but still does not attain the high light REE values of the older Mogollon and Echino groups.

We assume that variations in shale geochemistry are related to changing composition of source terrane rather than to changing weathering conditions. Al_2O_3, $CaO+N_2O$, K_2O (A–CN–K) relationships in shale provide an estimate of the degree of weathering of the source terrane before final deposition and burial (Fig. 15; Nesbitt & Young, 1989). With progressive weathering, major-element geochemistry of plutonic source rock shifts away from the CN apex and towards the A apex, as a function of feldspar weathering and mobile cation (Ca, Na) depletion (Nesbitt & Young, 1989). During early phases of weathering no relative loss of K_2O occurs. Throughout the Talara basin stratigraphy, shales exhibit a consistent degree of weathering (Fig. 15), enabling geochemical differences to be attributed to provenance rather than to climate and/or weathering changes.

Significant variations in REE fractionation throughout the Eocene stratigraphy is illustrated in Fig. 16. Shale units show significant shifts in REE mass fractionation (expressed by the ratio LaN/LuN; Rollinson, 1993) at major unconformities. The most notable shift from high (felsic) to low (mafic) fractionation occurs at the Echino–Talara contact.

DISCUSSION

Palaeogeographic evolution

The Lower Eocene section is characterized by a series of depositional systems ranging from terrestrial to shallow marine: Mogollon, Pale Greda/Ostrea, and Echino fms. (Fig. 3). The Mogollon Formation (Figs 3 and 4) is an alluvial fan to fluvial system transgressed by the overlying shallow marine Pale Greda Formation (Fildani, 2004). The Mogollon depositional system consists of a fluvial system in proximal areas (eastern portion of the basin), whereas equivalent shallow-marine facies can be found in the southern and western parts of the basin (Salinas-Mogollon Fm.; Fig. 6). A similar relationship is true for the Echino deltaic system and its shaly, deeper-water counterparts to the south (Fig. 6). With the exception of a gradual deepening of the Talara area to outer shelf or slope depths during Ostrea/Pale Greda deposition, water depths are generally shallow through the higher-order deltaic progradational cycles of the Echino Formation (Fig. 4). Fluvial and shallow marine sediment transport direction is consistently to the WNW, in accordance with the distribution of deeper water environments to the west (Fig. 17a).

A major palaeogeographic disruption is marked by the angular unconformity between the Echino and overlying Terebratula Formations, following uplift, tilting, and erosion of parts of the underlying sedimentary succession be-

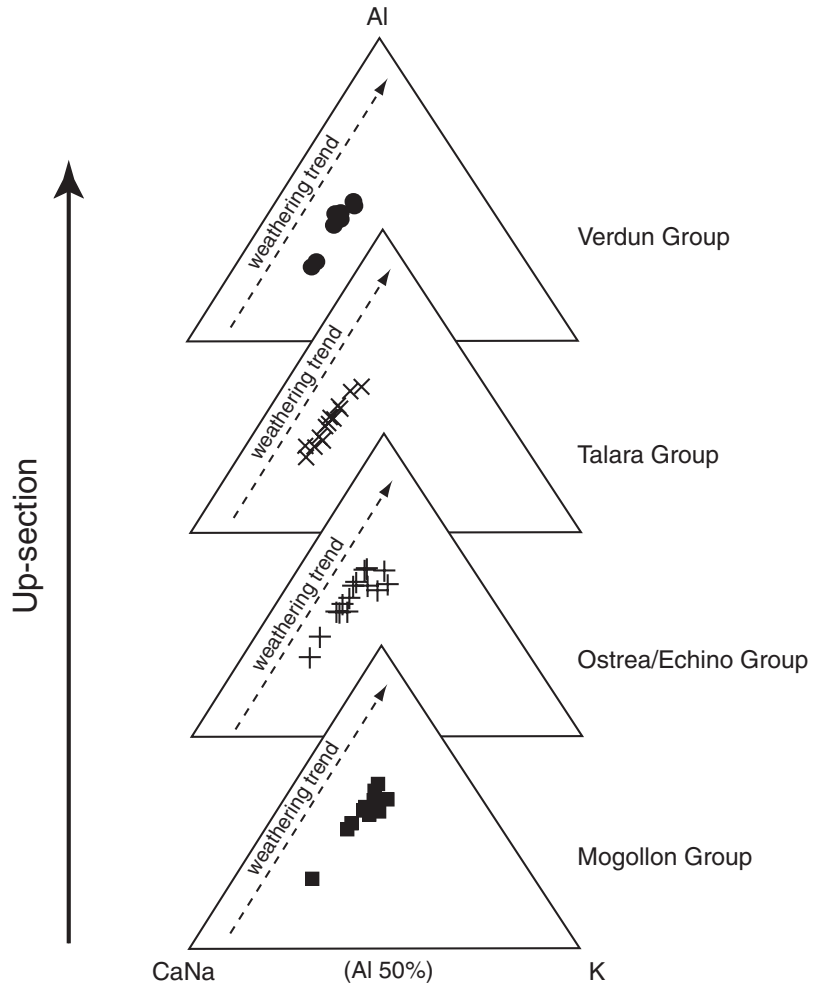

Fig. 15. Ca+Na, Al, K ternary diagrams for different shale groups to show that weathering trend did not affect Talara shale fractionation (Supplementary Table S1).

fore the major mid-Eocene deepening of the Talara basin. Subsurface data are in accordance; in at least one Perez Companc oil fields (Carrizo field in Block X), the Echino Formation is absent and the Talara Group is reported to unconformably overlie the Ostrea Formation (Gutierrez & Arriola, 2002).

Deepening of the middle Eocene shelf (Terebratula Formation) and deposition of the overlying deep-water (bathyal) shale (Lobitos Member, Talara Formation) is the first major phase of deep-water deposition in the Talara basin (Fig. 9b). The Talara Sandstone, which is comprised of highly discontinuous, lenticular sand bodies encapsulated in shales, is interpreted as the fill of channels that carved a palaeo-slope environment where the background deposition is represented by Talara Formation shale (Fildani, 2004) (Fig. 17). This palaeo-environment setting is similar to the modern slope described by Laursen & Normark (2003) and Spinelli & Field (2003). The channels filled by Talara Sandstone may have occurred between sub-basins where intervening ridges were covered by mud and fed by local sources from the shelf, either recycling shelf sand or bypassing the shelf and tapping into more distant sources (Fildani, 2004).

Basin configuration during this deepening event is uncertain due to likely lateral heterogeneities along the slope; however, palaeocurrent data suggest a westward sloping gradient (Figs 11 and 17). Abrupt changes in lateral facies associations encountered in the field suggest segmentation of the larger basin into sub-basins perhaps along major border faults.

The deep-water (bathyal) upper middle Eocene Pozo Formation shales cover the entire basin. This may be related to the shutting off of a distal coarse sediment supply during widespread deepening of the basin and/or to up-dip sequestration of the coarser material.

The ~1 m.y. hiatus proposed by Gutierrez & Arriola (2002) between the Pozo and Verdun Formations corresponds with a major palaeogeographic change at the boundary. The overlying Verdun Formation represents continued deposition into a deep-water setting but with a significant shift in sediment dispersal to the south (Figs 11 and 17). Sediment transport along the axis of a north–south elongated basin is in accordance with observations of the Verdun Formation extending to the southern Lancones basin (Fig. 2; Valencia & Uyen, 2002) and the Sechura basin (Dunbar *et al.*, 1990) as well as with subsurface indications of a north–south confining fault system (Gutierrez & Arriola, 2002; Picarelli *et al.*, 2003; Duerichen, 2005).

Deepwater sedimentation ended in the Talara basin by the upper Eocene, with deposition of the Chira Formation. Biofacies associations in the overlying Chira

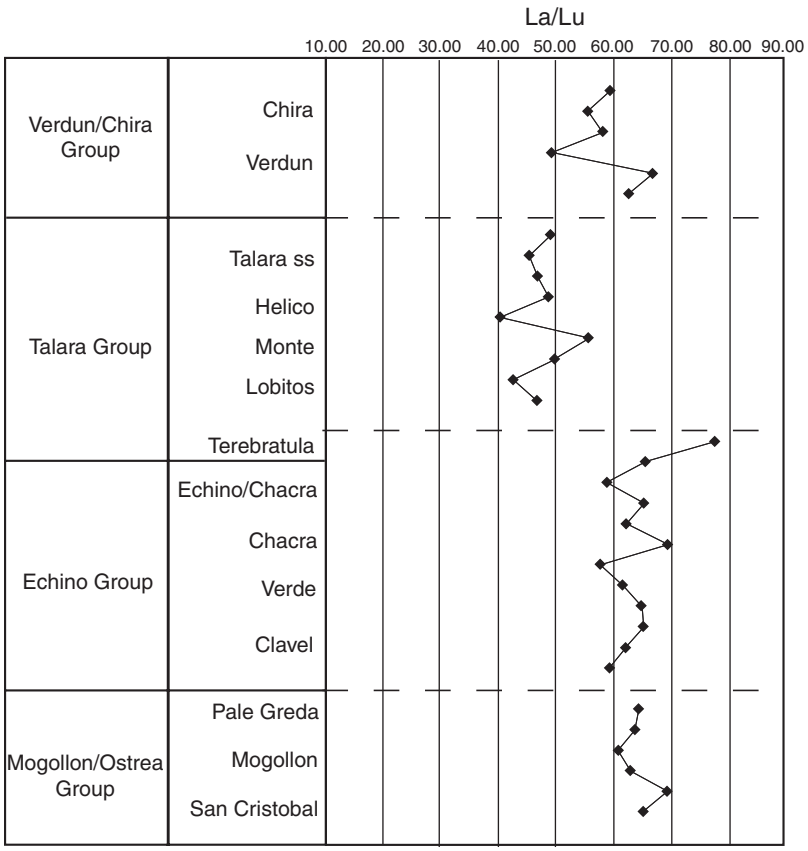

Fig. 16. La/Lu fractionation plot indicating variation of fractionation of rare-earth elements (REE) at major unconformities throughout the Eocene stratigraphy (data from supplementary Table S2).

Formation indicate a shoaling upward history (Fildani, 2004). By the time of deposition of the Oligocene Mancora Formation (Fig. 3), the basin was again characterized by shallow-marine water depths, with the Mancora sequence interpreted as a deltaic system (Kraemer *et al*., 1999). At that time, activity along the DGFS already controlled subsidence of the Tumbes basin as the locus of deposition shifted to the north (Fig. 2). The southern end of the Talara basin was uplifted in the late Oligocene as depocentres shifted northward, with upper Oligocene strata preserved only in the northern part of the basin (Fildani, 2004).

Provenance

The Mogollon Formation unconformably overlies the deformed Cretaceous and older rocks of the central and lowermost Amotape Mountains. This relationship suggests that the Amotape Mountains probably did not partition the Lancones and Talara basins during the lower Eocene Mogollon deposition, and that sediment from the Lancones basin did reach the Talara basin. The proximity of the Lancones basin to the east, and the SE–NW-directed palaeocurrents of the Mogollon Formation (Figs 11 and 17), suggest it may have been a significant source for the Talara basin. The petrography of the Mogollon sandstone, the clast composition of its conglomerate, and the overall geochemical signature of the shale and pebbles reflect a mixed source terrane (Figs 12, 13 and 14). Highly fractionated REE values of the shale indicate a strong felsic igneous component (Fig. 14). Sandstone petrography indicates an intermediate volcanic source area, and sandstone modes plot between the arc and recycled orogenic fields (Fig. 13a). The occurrence of a significant amount of intermediate volcanic detritus in the sandstone ($>10\%$) suggests the presence of a volcanic terrane among other sources. The Lancones basin does include a thick cover of Cretaceous (?) intermediate and basaltic volcanic flows (Valencia & Uyen, 2002). Recycled arc-derived materials from the Lancones basin may provide the partial arc and felsic signatures of Mogollon Formation sandstones and shales, respectively.

Above the Mogollon Formation, sandstone detrital modes of the Ostrea/Pale Greda formations continue to plot in the 'recycled orogenic' field with little influence from an Amotape-type source and only partial recycling of Cretaceous and lower Tertiary sandstone (Fig. 13d). The Lancones basin may have still been linked with the Talara basin through Pale Greda/Ostrea deposition. Detrital modes of the Cabo Blanco member (lowermost member of the Echino group), however, indicate a mature sandstone mainly composed of medium- to well-rounded monocrystalline quartz, which also plots very closely with the Palaeocene Amotape-derived Basal Salina sandstone (Marsaglia & Carozzi, 1991). We infer that the Amotape Mountains were a topographic high at this time, isolating the Talara basin from the Lancones basin and serving as a primary sediment source for the Echino Formation. This potential Amotape uplift corresponds with renewed

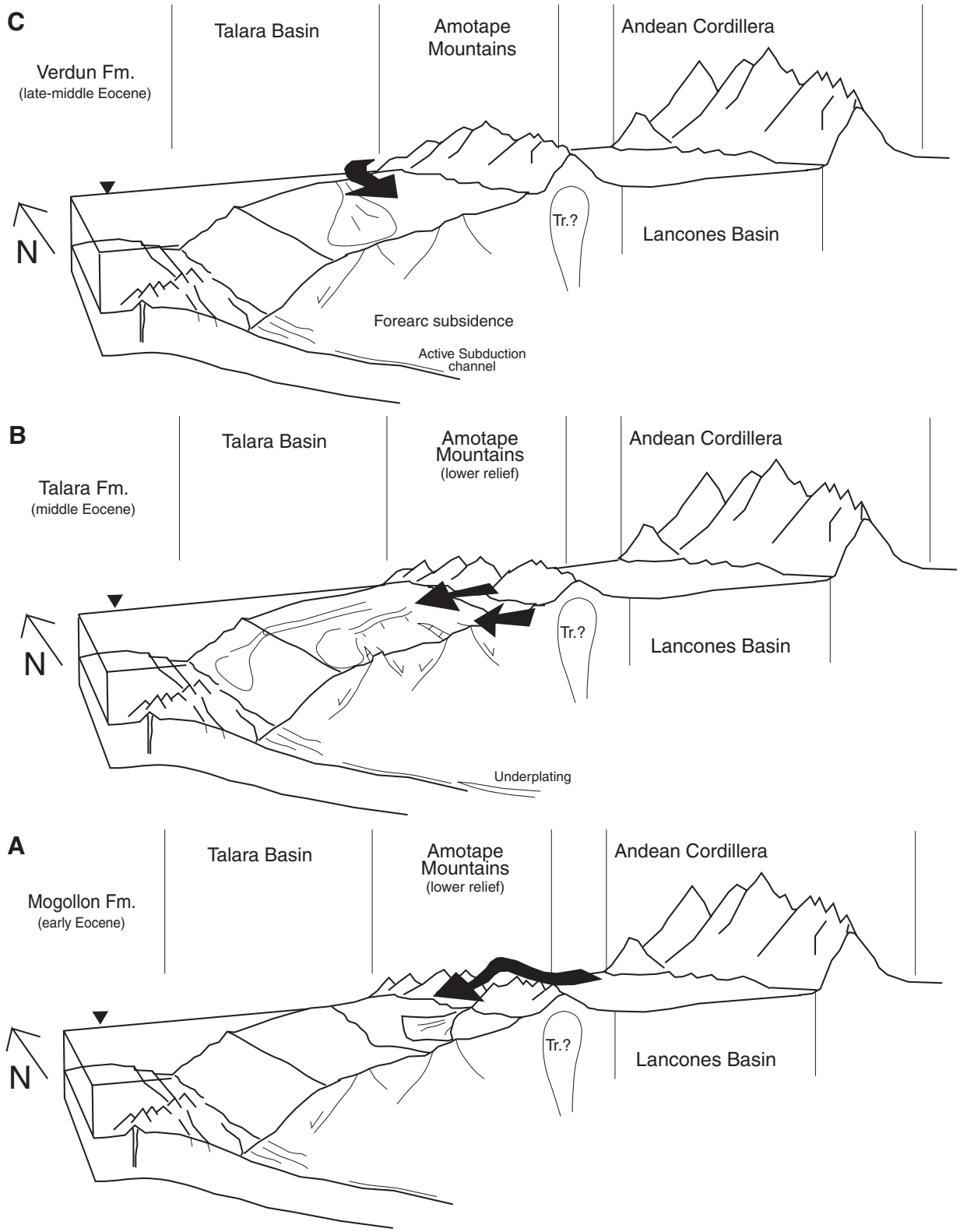

Fig. 17. Block diagram summarizing the different stages of Talara basin evolution during the Eocene. Arrows indicate gross palaeo-dispersal patterns (see details Fig. 11). (A) In the early Eocene (Mogollon time) sediments from the Lancones basin were able to bypass the Amotape Mountains. Mogollon Fm. palaeo-dispersal patterns indicate northwestward directions with sediments wedging out eastward. (B) By the middle Eocene (Talara time), the basin is highly partitioned with areas of deep-water sedimentation. Palaeo-dispersal patterns are more mature with diverse sources (mixed Amotape sources and Lancones-related detritus able to bypass the Amotape Mountains to the south - see Fig. 11 for details). (C) By the late middle Eocene (Verdun time) the dominant palaeo-dispersal pattern is towards the south with the Amotape Mountains separating the fully deep-water Talara basin from the Lancones basin to the east. Diagram inspired by Shepherd & Moberly, 1981.

east–west deltaic progradation of the Echino Formation onto the outer shelf environment of the Pale Greda/Ostrea Formations.

The late-Middle Eocene Terebratula Formation rests with angular unconformity on the Echino Formation and shows a marked shift towards more lithic-rich sandstone (Fig. 13b) and a more mafic source terrane (Fig. 16). The presumed uplift and erosion associated with the angular discordance may have provided the increased lithic component in Terebratula sandstone. As well, the onset of Talara Formation deep-water sedimentation above the Terebratula Formation corresponds with a significant shift in detrital composition. Sandstone, conglomerate, and shale of the Talara Group indicate a more intermediate volcanic (or partly mafic) source (Figs 12–14). Talara shale REE reflects a partly mafic source terrane (Fig. 14); sandstone detrital modes of the Helico sandstone also indicate a source enriched with intermediate to mafic volcanic material (Fig. 13). The palaeogeographic model proposed here for the Talara Formation includes a westward-dipping incised slope system, possibly partitioned into fault-controlled sub-basins. Possible intermediate- to mafic-volcanic source areas could be either the arc to the east, the Raspas Group to the north (Fig. 2; Arculus *et al*., 1999; Spikings *et al*., 2005), or the Lancones basin to the east, if sediment was again able to bypass the Amotape barrier. If the Talara deepening event was regional, and subsidence involved the entire forearc region, perhaps the Amotape Mountains were a lower relief feature and sediment from Lancones basin was able to reach the outboard basin of Talara (Fig. 17). Work from Duerichen (2005) indicates that palaeocurrents of the Helico Member have dominantly northwestward directions indicating the Lancones basin as a very promising source area (Fig. 11). We cannot discount that the largely unmapped Cordillera to the east may have contributed arc-related detritus, bypassing the Lancones basin. Preliminary detrital zircon data indicate presence of an active arc throughout the Eocene (Hessler & Fildani, 2005).

Another shift in sediment composition and in palaeocurrent dispersal pattern is evident in the late middle Eocene Verdun Formation; a highly fractionated (felsic) REE signature (Figs 14 and 16), the sandstone composition (Fig. 13), the presence of meta-granodioritic cobbles (Fig. 12), and north–south palaeocurrents (Fig. 11) set this formation apart from the underlying Talara Formation. The presence of sandstone cobbles in the Verdun Formation, which contain the same Verdun index microfossils (*Lepidocyclina peruviana*), suggest partial recycling of the Verdun Formation itself. The Verdun Formation is recognized across the entire basin, but with the more distal facies in the southern basin (Fildani, 2004; Duerichen, 2005). This palaeogeography, together with the occurrence of intraformational clasts, indicate that inversion occurred in the north, where Verdun beds were uplifted, eroded, and recycled into the southern part of the basin. The ~1 m.y. hiatus between the Talara Group and the Verdun Formation indicated by Gutierrez & Arriola (2002) may have specifically involved partial uplift and erosion of the Eocene strata of the northern end of the basin in the late Eocene.

During the early Oligocene, the locus of deposition shifted to the north with deposition of the thick fluvio-deltaic sequence of the Mancora Formation spilling into the Tumbes basin (Kreamer *et al*., 1999; Fildani, 2004; Fildani *et al*., 2005). The Mancora Formation sediments suggest a shift to more 'mafic' source material with the presence of andesitic cobbles in the conglomerate (Fildani, 2004). Shale geochemistry confirms a shift to mafic sources that could be the geographically nearby Raspas Complex (Table S1; Fig. 2).

Basin tectonics

Evolution of the Talara basin is directly tied to regional interactions between the South American and Farallon-Nazca plates. However, the peculiar forearc position, with a modern quiescent arc (Andean Cordillera), escape tectonics features to the north (DGFS and Gulf of Guayaquil), and the present day flat-slab subduction (Bernal *et al*., 2002) make for a complicated tectonic reconstruction of the basin's Eocene history.

Eocene deep-water deposition in the Talara basin is unique relative to other coastal basins of northern Peru and southern Equador, which are characterized by shallow-marine deposition or non-deposition during the late Eocene (Jaillard *et al*., 1995; Jaillard & Soler, 1996). This abrupt deepening (~1000 m of bathymetric change) is almost one order of magnitude greater than global eustatic sea-level fluctuations (Hardenbol *et al*., 1998) that occurred within the same time frame, emphasizing its tectonic driver (Fig. 4). Moreover, eustatic fluctuations are dominantly regressive during this time interval, requiring significantly enhanced, tectonically driven subsidence (Fig. 4). The mechanisms behind these deep-water events are not clear, but they are probably related to a combination of wrench tectonism and subduction erosion. Eustacy appears to have played a minor role in sedimentation in Talara basin.

Wrench tectonics may be manifest in the origin and behaviour of the Amotape–Tahuin block. The tectonics are more complicated than the simplistic scenario that proposes the Amotape–Tahuin block as accreted to South America (Feininger, 1987; Mourier *et al*., 1988). The Amotape–Tahuin Block north of the Naranjo Fault zone is composed of a regional-scale mélange which encloses tectonic blocks of high-pressure, low-temperature rocks interpreted as a partially subducted and now exhumed oceanic assemblage of an accretionary prism (Fig. 2; Arculus *et al*., 1999; Spikings *et al*., 2005, among others). The Amotape–Tahuin block south of the Naranjo fault is a continental block that rotated clockwise as consequence of multiple terrane collisions along the Ecuadorian margin (Spikings *et al*., 2005). Cooling and rotation of the block at 43–39 Ma could be directly related to the collision of the Macuchi Island Arc with the Ecuadorian margin (Spikings *et al*., 2005). Recently published ages from granitoids in the

Amotape Mountains indicate a Triassic crystallization age related to the break-up of western Gondwana (Jaillard *et al*., 1990; Noble *et al*., 1997) and continental affinities for the S-type, granitoid intrusions of the Tres Lagunas block in Ecuador (Sanchez *et al*., 2006) suggesting its para-autochthonous origins as a translated sliver of the Cordillera Real (Aspden & Litherland, 1992; Aspden *et al*., 1992; Spikings *et al*., 2005).

Rotation of the Amotape–Tahuin block during the Late Cretaceous–early Tertiary (Mourier *et al*., 1988; Jaillard *et al*., 1999) and more specifically in the late Eocene (Spikings *et al*., 2005) indicates that coeval wrench tectonism was active in the Talara forearc region as terrane collisions affected the plate boundary. The change in palaeo-dispersal patterns and possible uplift in the northern source areas during Verdun time deposition could be related to terrane collision along the Ecuadorian margin (Spikings *et al*., 2005). Evidence for right-lateral strike–slip movement is reported for the Dolores–Guayaquil system from the Miocene to recent (Kreamer *et al*., 1999) but may have occurred earlier based on the presumed mid-Eocene uplift of the Amotape–Tahuin block that served to isolate the Talara and Lancones basins (Fig. 17). Large-scale strike–slip faulting can result in rapid vertical tectonism and lateral shifting along the boundary of large and small blocks over distances of hundreds of kilometres (Ryan & Coleman, 1992); resultant deep, partitioned basins create high accommodation space for sudden deep-water deposition and rapid lateral facies changes, as is seen in the mid-Eocene Talara section (Figs 4 and 17). During this time the Amotape block was segmented and partially submerged.

As a modern analogue, right-lateral motion is behind the formation of the northern Progreso-Tumbes basins. Witt *et al*. (2006) reported evidence of large-scale extensional faults accommodating the thick sedimentary fill in the Gulf of Guayaquil (Witt *et al*., 2006). The recent rapid opening of the Gulf is explained by escape tectonism and northward movement of the North Andean Block (Witt *et al*., 2006), but the area was already a locus of sedimentation during the Oligocene (Mancora Formation of Tumbes basin; Fildani, 2004) and the Miocene (Progreso basin; Kreamer *et al*., 1999).

Another mechanism for Eocene subsidence could be extension related to subduction erosion (*sensu* Von Heune & Scholl, 1991). This mechanism may have caused the regional forearc deepening during Verdun deposition (Fig. 17). Sediment accretion, sediment subduction, and subduction erosion seem to take place at the same time along the western margin of South America (Sage *et al*., 2006). Basal subduction erosion of the forearc crustal basement inboard of an accretionary prism is quite common (see review in Clift & Vannucchi, 2004) and deep-water forearc basins may form as a result of enhanced thinning of the upper plate through basal subduction erosion along the plate interface, as explained by Laursen & Normark (2003). For example, subsidence of the Lima basin is controlled by subduction erosion related to the subducting Nazca plate underneath South America causing hundreds of metres of vertical excursion in the forearc position (Clift *et al*., 2003).

Sediment in the trench seems to play a major role in 'lubrication' of the subduction channels controlling intraplate coupling and de-coupling. Forearc basins can form due to subduction erosion even in overfilled trenches (Wells *et al*., 2003). It is worthwhile to explore the possibility that enhanced trench-filling caused by wrench tectonism during 'Talara Formation time' may have locked the intraplate zone, thereby forcing subduction erosion and subsequent regional deepening during 'Verdun Formation time' (Fig. 17). In any case, we speculate that locking and unlocking related to variable coupling in the intraplate position causes extensile or contractile phases (as reported in Bourgois *et al*., 2007), resulting in dramatic vertical forearc movements such as that observed in the Eocene Talara basin (this study) or in the Lima Basin (Clift *et al*., 2003).

Modern subduction erosion along the Peruvian trench is well documented (Clift *et al*., 2003) even at Talara basin's latitude (Bourgois *et al*., 2007). Bourgois *et al*. (2007) documented major detachment faults offshore of Talara and speculated on their direct connection with the subduction channel. Local events in the trench, such as subduction of seamounts, could cause major erosion underneath the overriding plate and enhance the extensional fabric in the forearc region. The Talara basin may have evolved in a Valparaiso basin-type setting (*sensu* Laursen & Normark, 2003), very similar to that associated with Carnegie ridge subduction occurring off the modern coast of Ecuador (Fig. 2).

Subduction erosion events in the Talara basin correspond with and may have been enhanced by the late Middle Eocene contractional Inca II tectonic phase (Jaillard *et al*., 1995; Benavides-Caceres, 1999). Plate rearrangement and changes in convergence rate would encourage subduction erosion with subsidence in the upper plate and major sediment accumulation in the forearc position (Fig. 4) (Fildani, 2004).

We speculate that the modern Talara basin is what remains of a once much larger forearc basin. Bourgois *et al*. (2007) estimated that subduction erosion removed $\sim$25 to 100 km^3 Myr km^{-1} for the past $\sim$5.2 Myr. The presence of Precambrian and Palaeozoic basement in the Ciclayo canyon on the Peruvian slope just south of the study area (Sosson *et al*., 1994) confirms subduction erosion along this margin possibly for even longer periods.

Today, flat-slab subduction, collision and partial subduction of seamounts into the Peruvian trench (Fig. 1), as well as intensified coupling along subduction channels caused by intraplate locking (Bourgois *et al*., 2007), all combine to cause dramatic vertical excursions the Talara region. Emergent Pleistocene terraces show up to $\sim$400 m of uplift along the Talara coast (Pedoja *et al*., 2006; Bourgois *et al*., 2007), and this uplift has been linked to the Carnegie ridge subduction (Pedoja *et al*., 2006) and to poor lubrication and locking along the subduction channel in the intraplate position (Bourgois *et al*., 2007).

CONCLUSIONS

The Eocene section of Talara basin records rapid shifts of depositional, stratigraphic and provenance patterns. Deposition in terrestrial to shallow-marine environments persisted until the abrupt deepening of the basin starting in the Middle Eocene. This deepening event loosely corresponds with a reported change in the direction of plate convergence (Pardo-Casas & Molnar, 1987; Somoza, 1998). Reorganization of plate motion vectors and new convergence direction may have enhanced subduction erosion of the overriding plate (*sensu* Clift *et al.*, 2003) or wrench tectonism and reactivated strike–slip faults that were active during the Late Cretaceous, causing the major extension in the Late Middle Eocene that correspond to the deposition of the deep-water sequences of the Talara Formation. Stratigraphic and provenance data suggest a direct relationship between sedimentary packaging and regional tectonics with changes in source terranes and sediment dispersal patterns at major unconformities. A sharp shift is recognized at the onset of deep-water sedimentation within the Talara Formation (Lobitos shale Member) by an increased influx of mafic material to the basin related to the segmentation and partial subsidence of the Amotape Block. A later deepening phase is reflected by the deposition of the deep-water Verdun Formation that shows a different dispersal pattern than the Talara Formation and was deposited after a hiatus of $\sim$1 Ma (Gutierrez & Arriola, 2002). The active wrench tectonism of the 'Talara Formation time' may have favored the sediment delivery in the trench, initially locking and eventually lubricating and unlocking the intraplate zone, thereby forcing subduction erosion and subsequent regional deepening during 'Verdun Formation time'. Locking and unlocking related to variable coupling in the intraplate position causes extensile or contractile phases (as reported in Bourgois *et al.*, 2007), possibly resulting in vertical forearc movements such as the ones observed in the Eocene of Talara basin. Variation of intraplate coupling and partial locking of subduction plates have been identified as some of the major causes behind switching tectonic setting from contraction to extension (and vice versa) in the forearc region. Collisions of terranes along the Ecuadorian margins (Spikings *et al.*, 2005) forced inversion of the basin starting in the late Eocene (Verdun time). Eventually active deposition shifted to the north in the modern Gulf of Guayaquil area. Talara basin sedimentary fill is thus the result of a complicated forearc history: it was never completely isolated from surrounding basins and its configuration and sediment source areas changed through time. The Amotape–Tahuin block was not a persistent barrier between the Talara basin and the arc area, and so arc-derived detritus was able to reach the basin episodically.

ACKNOWLEDGEMENTS

We thank Perez Companc del Peru (now Petrobras del Peru) for financial support and help in the field. In particular, A. F. would like to thank the geologists of Perez Companc del Peru (Pedro Raul Arriola, Gerardo Pozo, Peter 'Pedro' McGregor, the late Juan Leyva, Fabian Gutierrez, Ricardo Savini, Jose Daudt and many others) that helped to improve our understanding of the basin through discussions about the geology of NW Peru. This manuscript is solidly built on the results of two PhD dissertations supported by Perez Companc and based on extensive field mapping and facies analysis, integrated with proprietary unpublished subsurface data (Fildani, 2004; Duerichen, 2005). Erin Duerichen is thanked for sharing ideas. Special thanks go to SPODDS (Stanford Project On Deep-water Depositional Systems), a consortium of 15 oil-companies. Bill Normark, Don Lowe and Jim Ingle are thanked for reviewing early versions of this manuscript. Constructive comments from Reviewers Kathie Marsaglia, Jeff Trop, Dave Scholl and Editor Peter DeCelles largely improved this manuscript. Agustin Cardona and Anthony Tankard are thanked for insightful conversations about the general tectonic setting of South America. Brad Ritts (Chevron) is thanked for reading the latest version of this paper.

A. F. and A. M. H would like to dedicate this manuscript to their son Cesare, whose arrival joyfully delayed this publication.

Supplementary Material

The following material is available for this article online:

Table S1. Major and trace element data for shales in the Talara Basin. XRF analyses performed by Washington State GeoAnalytical Laboratories.

Table S2. Unnormalized rare-earth element data for shales in the Talara Basin. ICP-MS analyses performed by Washington State GeoAnalytical Laboratories.

This material is available as part of the online article from: http://www.blackwell-synergy.com/doi/abs/10.1111/j.1365-2117.2007.00346.x (This link will take you to the article abstract).

Please note: Blackwell Publishing are not responsible for the content or functionality of any supplementary materials supplied by the authors. Any queries (other than missing material) should be directed to the corresponding author for the article.

REFERENCES

Arculus, R.J., Lapierre, H. & Jaillard, E. (1999) Geochemical window into subduction and accretion processes: Raspas metamorphic complex, Ecuador. *Geology*, **27**(6), 547–550.

Aspden, J.A., Fortey, N., Litherland, M., Viteri, F. & Harrison, S.M. (1992) Regional S-type granites in the Ecuadorian Andes: possible remnants of the break-up of western Gondwana. *J. South Am. Earth Sci.*, **6**, 123–132.

Aspden, J.A. & Litherland, M. (1992) The geology and Mesozoic collisional history of the Cordillera Real, Ecuador. *Tectonophysics*, **205**, 187–204.

Bellido, B.E. (1969) Synopsis de la Geologia del Peru. *Serv. Geol. Miner., Peru, Boletin*, **22**, 1–54 (in Spanish).

Benavides-Caceres, V. (1999) Orogenic evolution of the Peruvian Andes; the Andean Cycle. In: *Geology and Ore Deposits of the Central Andes* (Ed. by B.J. Skinner), *Spec. Publ.–Soc. Econ. Geol.*, **7**, 61–107.

Berggren, W.A., Kent, D.V., Swicher III, C.C. & Aubry, M.P. (1995) A revised cenozoic geochronology and chronostratigraphy. In: *Geochronology, Time Scales and Global Stratigraphic Correlation* (Ed. by W.A. Berggren, D.V. Kent, M.P. Aubry & J. Hardenbol), *Soc. Sediment. Geol., Spec. Publ.* **54**, 129–212.

Bernal, I., Tavera, H. & Antayhua, Y. (2002) Zonas sismogenica en el Peru: volumenes de informacion, graficos polares y zonificacion preliminary. *Bol. Soc. Geol. Peru*, **93**, 31–44.

Bosworth, T.O. (1922) *Geology of the Tertiary and Quaternary Periods in the Northwest Part of Peru*. Macmillan and Company, London, UK, 434pp.

Bouma, A.H. (1962) *Sedimentation of Some Flysch Deposits*. Elsevier, Amsterdam, 168pp.

Bourgois, J., Bigot-Cormier, F., Bourles, D., Braucher, R., Dauteuil, O., Witt, C. & Michaud, F. (2007) Tectonic record of strain buildup and abrupt co-seismic stress release across the northwestern Peru coastal plain, shelf, and continental slope during the past 200 kyr. *J. Geophys. Res.*, **112**, BO4104, doi:10.1029/2006JB004491.

Bush, V.A., Vinogradov, L.D. & Titov, A.I. (1994) Tectonic breccia and thrust tectonic of the tertiary deposits in northwestern Peru. *Geotectonic (English translation)*, **28**, 159–167.

Caldas, J., Palacios, O., Pecho, V. & Vela, C. (1980) Geologia de los Cuadrangulos de: Bayovar, Sechura, La Retonda, Pta. la Negra, Lobos de Tierra, Las Salinas y Morrope. *Inst. Geolog. Miner. Metal. Bol., Ser. A*, **32**, 1–78.

Carozzi, A.V. & Palomino, J.R. (1993) The Talara forearc basin: depositional models of oil-producing Cenozoic clastic systems. *J. Petrol. Geol.*, **16**(1), 5–32.

Chew, D.M., Scheltegger, U., Košler, J., Whitehouse, M.J., Gutjahr, M., Spikings, R.A. & Miškovic, A. (2007) U-Pb geochronologic evidence for the evolution of the Gondwanan margin of the north-central Andes. *Geol. Soc. Am. Bull.*, **119**, 697–711.

Clift, P.D., Pecher, I., Hutt, L., Kukowski, N. & Hampel, A. (2003) Tectonic erosion of the Peruvian forearc, Lima Basin, by subduction and Nazca Ridge collision. *Tectonics*, **22**, 1023.

Clift, P.D. & Vannucchi, P. (2004) Controls on tectonic accretion versuserosion in subduction zones: implications for the origin and recycling of the continental crust. *Rev. Geophys.*, **42**, RG20001, doi: 10.1029/2003RG000127.

Cullers, R., DiMarco, M., Lowe, D.R. & Stone, J. (1993) Geochemistry of a silicified, felsic volcanic suite from the early Archean Panorama Formation, Pilbara Block, western Australia; an evaluation of depositional and post-depositional processes with special emphasis on the rare-earth elements. In: *Archean and Early Proterozoic Geology of the Pilbara region, Western Australia* (Ed. by T. Blake & A. Meakins), *Precambr. Res.*, **60**, 1–4, 99–116.

Daudt, J.A., Grosso, S. & Sullivan, M.D. (2004) Sea-level changes and tectonic influence in the deposition of the Cabo Blanco Member: example of an Eocene fluvio-estuarine system in Talara basin, NW Peru. *Bol. Soc. Geol. Peru*, **97**, 67–80.

DeVries, T.J. (1988) The geology of late Cenozoic marine terraces (tablazos) in northwestern Peru. *J. South Am. Earth Sci.*, **1**, 121–136.

Dickinson, W.R. (1970) Interpreting detrital modes of greywacke and arkose. *J. Sediment. Petrol.*, **40**, 695–707.

Dickinson, W.R. (1985) Interpreting provenance relations from detrital modes of sandstones. In: *Provenance of Arenites* (Ed. by G. Zuffa), pp. 333–361. D. Reidel, Dordrecht.

Dickinson, W.R. (1995) Forearc basins. In: *Tectonics of Sedimentary Basins* (Ed. by C.J. Busby & R.V. Ingersoll), pp. 221–261. Blackwell Scientific Publications, Oxford.

Duerichen, E. (2005) Sedimentology and architecture of upper Eocene deep-water deposits, Talara basin, NW Peru. PhD Thesis, Stanford University.

Dunbar, R.B., Marty, R.C. & Baker, P.A. (1990) Cenozoic marine sedimentation on the Sechura and Pisco basins, Peru. *Palaeogeogr. Palaeoclimatol. Palaeoecol.*, **77**, 235–261.

Feininger, T. (1987) Allochthonous terranes in the Andes of Ecuador and northwestern Peru. *Can. J. Earth Sci.*, **24**, 266–278.

Fildani, A. (2004) Analysis of two arc-associated basins and onset of their deep-water stages: Magallanes basin, Chile, and Talara Basin. Peru. PhD Thesis, Stanford University, Stanford, California, p. 375.

Fildani, A., Hanson, A.D., Chen, Z., Moldowan, M.J., Graham, S.A. & Arriola, P.R. (2005) Talara basin petroleum system: geochemical characteristics of oils and correlation with possible source rocks from NW Peru. *Am. Assoc. Petrol. Geol. Bull.*, **89**, 1519–1545.

Gonzales, G. (1976) Ciclo de sedimentation en el Eocene de la cuenca Talara. *Bol. Soc. Geol. Perú*, **51**, 73–80.

Gutierrez, F.E. & Arriola, I.P. (2002) Analisis estratigrafico de los ciclos Talara-Verdun para la generacion de nuevas oportunidades–Yacimento Carrizo–Cuenca Talara–Peru. INGEPET, EXPR-3-FG-33. (Extended Abstract, non peer reviewed, in Spanish).

Gutscher, M.A., Malavieille, J., Lallemand, S. & Collot, J.-Y. (1999a) Tectonic segmentation of the North Andean margin: impact of the Carnegie Ridge collision. *Earth Planet. Sci. Lett.*, **168**, 255–270.

Gutscher, M.A., Olivet, J.L., Aslanian, D., Eissen, J.P. & Maury, R. (1999b) The "lost Inca Plateau": cause of flat subduction beneath Peru? *Earth Planet. Sci. Lett.*, **171**, 335–341.

Hardenbol, J., Thierry, J., Farley, M.B., Jacquin, T., De Graciansky, P.C. & Vail, P.R. (1998) Mesozoic-Cenozoic sequence chronostratigraphic chart. In: *Mesozoic and Cenozoic Sequence Stratigraphy of European Basins* (Ed. by P.C. De Graciansky, J. Hardenbol, T. Jacquin, P.R. Vail & M.B. Farley), *SEPM Spec. Publ.*, **60** (charts).

Hessler, A.M. & Lowe, D.R. (2006) Weathering and sediment generation in the Archean: An integrated study of the evolution of siliciclastic sedimentary rocks of the 3.2 Ga Moodies Group, Barberton Greenstone Belt, South Africa. *Precambrian Research*, **151**, 185–210.

Hessler, A.M. & Fildani, A. (2005) Detrital zircon geochronology as applied to the evolution of the petroleum-rich Talara basin, northwest Peru. *Geol. Soc. Am. Abstr. Programs*, **37**, 4–51.

Iddings, A. & Olsson, A. (1928) Geology of northwest Peru. *Am. Ass. Petrol. Geol. Bull.*, **12**, 1–39.

INGEMMET (Instituto Geologico Minero Y Metalurgico Del Peru). (1999) Bolletin Numero 55, Serie A: Carta Geologica Nacional (1:100000). Responsable Oscar Palacios Moncayo, Lima. http://www.ingemmet.gob.pe/Images/productos/imagenes_asociadas/Publicaciones.pdf

Ingersoll, R.V., Bullard, T.F., Ford, R.L., Grimm, J.P., Pickle, J.D. & Sares, S.W. (1984) The effect of grain size on

detrital modes: a test of the Gazzi-Dickinson point-counting method. *J. Sediment. Petrol.*, **54**, 103–116.

Ingle, J.C. Jr. (1980) Cenozoic paleobathymetry and depositional history of selected sequences within the southern California continental borderlands. *Cushman Foundation Foraminiferal Res. Spec. Publ.*, **19**, 165–195.

Ingle, J.C. Jr., Keller, G. & Kolpack, R.L. (1980) Benthic foraminiferal biofacies, sediments and water masses of the southern Peru-Chile Trench area, southeastern Pacific Ocean. *Micropaleontology*, **26**(2), 113–150.

Jaillard, E., Herail, J., Monfret, T., Diaz-Martinez, E., Baby, P., Lavenu, A. & Dumont, J.F. (2000) Tectonic evolution of the Andes of Ecuador, Peru, Bolivia, and northernmost Chile. In: *Tectonic Evolution of South America* (Ed. by U.G. Cordani, E.J. Milani, A.T. Filho & D.A. Campos), pp. 481–561. 31st International Geological Congress, Rio de Janeiro.

Jaillard, E., Laubacher, G., Bengtson, P., Dhondt, A.V. & Bulot, L.G. (1999) Stratigraphy and evolution of the Cretaceous forearc Celica-Lancones basin of the southwestern Equador. *J. South Am. Earth Sci.*, **12**, 61–68.

Jaillard, E., Ordonez, M., Benitez, S., Berrones, G., Jimenez, N., Montenegro, G. & Zambrano, I. (1995) Basin development in an accretionary, oceanic-floored forearc setting: southern coastal Ecuador during late Cretaceous to Late Eocene times. In: *Petroleum Basins of South America* (Ed. by A.J. Tankard, R. Suarez Soruco & H.J. Welsink), *Am. Ass. Petrol. Geol. Mem.*, **62**, 597–613.

Jaillard, E. & Soler, P. (1996) Cretaceous to early Paleogene tectonic evolution of the northern Central Andes (0–18°S) and its relations to geodynamics. *Tectonophysics*, **259**, 41–53.

Jaillard, E., Soler, P., Carlier, G. & Mourier, T. (1990) Geodynamic evolution of the northern and central Andes during early to middle Mesozoic times: a Tethyan model. *J. Geol. Soc. London*, **147**, 1009–1022.

Kraemer, P., Weiner, G. & Alvarez, P. (1999) Evolucion Tectonoestratigrafica de la Cuenca de Tumbes-Progreso, offshore Peru. INGEPET, EXPR-1-PK-07. (Extended abstract, non peered review, in Spanish).

Lamb, S. & Davis, P. (2003) Cenozoic climate change as a possible cause for the rise of the Andes. *Nature*, **425**, 792–797.

Laursen, J. & Normark, W.R. (2003) Impact of structural and autocyclic basin-floor topography on the depositional evolution of the deep-water Valparaiso forearc basin, central Chile. *Basin Res.*, **15**, 201–226.

Lonsdale, P. (1978) Ecuadorian subduction system. *Am. Ass. Petrol. Geol. Bull.*, **62**, 2454–2477.

Lowe, D.R. (1982) Sediment gravity-flows II; depositional models with special reference to the deposit of high-density turbidity currents. *J. Sediment.Petrol.*, **52**, 279–297.

Marsaglia, K.M. & Carozzi, A.V. (1991) Depositional environment, sand provenance, and diagenesis of the basal salina formation (lower Eocene), NW Peru. *J. South Am. Earth Sci.*, **3**, 253–267.

Mayes, C.L., Lawver, L.A. & Sandwell, D.T. (1990) Tectonic history and new Isochron chart of South Pacific. *J. Geophys. Res.*, **95**, 8543–8567.

McLennan, S.M. (1989) Rare earth elements in sedimentary rocks, influence on provenance and sedimentary processes. In: *Geochemistry and Mineralogy of Rare Earth Elements* (Ed. by B.R. Lipin & G.A. McKay), *Rev. Mineralogy*, **21**, 169–200.

Mourier, T., Laj, C., Megard, F., Roperch, P., Mitouard, P. & Farfan Medrano, A. (1988) An accreted continental terrane in northwestern Peru. *Earth Planet. Sci. Lett.*, **88**, 182–192.

Nesbitt, H.W. (1979) Mobility and fractionation of rare earth elements during weathering of a granodiorite. *Nature*, **279**, 206–210.

Nesbitt, H.W. & Young, G. (1989) Formation and diagenesis of weathering profiles. *J. Geol.*, **97**, 129–147.

Noble, S.R., Aspden, J.A. & Jemielita, R. (1997) Northern Andean crustal evolution: new U-Pb geochronological constraints from Ecuador. *Geol. Soc. Am. Bull.*, **109**, 789–798.

Noblet, C., Lavenu, A. & Marocco, R. (1996) Concept of continuum as opposed to periodic tectonism in the Andes. *Tectonophysics*, **255**, 65–78.

Nurnberg, D. & Muller, R.D. (1991) The tectonic evolution of the South Atlantic from late Jurassic to present. *Tectonophysics*, **191**, 27–53.

Okada, H. & Bukry, D. (1980) Supplementary modification and introduction of code numbers to the lower latitude coccolith biostratigraphic zonation (Bukry, 1973, 1975). *Mar. Micropaleontol.*, **5**(3), 321–325.

Palomino, J.R. & Carozzi, A.V. (1979) Sedimentology and electric log interpretation of the Cabo Blanco Sandstone (Lower Eocene), Talara basin, northwest Peru. *Archives des Sciences, Societe de Physique et d'Histoire Naturelle de Geneve*, **32**, 127–149.

Pardo-Casas, F. & Molnar, P. (1987) Relative motion of the Nazca (Farallon) and South American plates since late Cretaceous time. *Tectonophysics*, **6**, 233–248.

Pedoja, K., Ortlieb, L., Dumont, J.F., Lamothe, M., Ghaleb, B., Auclair, M. & Laborusse, B. (2006) Quaternary coastal uplift along the Talara Arc (Ecuador, Northern peru) from new marine terrace data. *Mar. Geol.*, **228**, 73–91.

Picarelli, A.T., Pozo, E.G., Daudt, J., Leyva, J., Arriola, P. & Arispe, A. (2003) Upper-Eocene Fault-Controlled Deep Water Systems in the Talara Forearc Basin, Northwest Peru: Sand-Transport Paths, Sand-Body Geometry and Exploration and Development Opportunities. AAPG Abstract, AAPG Annual Meeting, May 11–14, 2003.

Reynaud, C., Jaillard, E., Lapierre, H., Mamberti, M. & Mascle, G.H. (1999) Oceanic plateau and island arcs of southwestern Ecuador: their place in the geodynamic evolution of northwestern South America. *Tectonophysics*, **307**, 235–254.

Rollinson, H. (1993) *Using Geochemical Data: Evaluation, Presentation, Interpretation*. Prentice Hall, Pearson Education Limited, Longman Group, London, UK, 352pp.

Ryan, H.F. & Coleman, P.J. (1992) Composite transform-convergent plate boundaries: description and discussion. *Mar. Petrol. Geol.*, **9**, 89–97.

Sage, F., Collot, J.-Y. & Ranero, C.R. (2006) Interplate patchiness and subduction-erosion mechanisms: evidence from depth-migrated seismic images at the Central Ecuador convergent margin. *Geology*, **34**, 997–1000.

Sanchez, J., Palacios, O., Feininger, T., Carlotto, V. & Quispesivana, L. (2006) Puesta en evidencia de granitoides triasico an loa Amotape-Tahuin: Deflexion de Huancabamba. XIII Congreso Peruano de Geologia, Resumenes Extendidos, Sociedad Geologica del Peru, pp. 312–315. (Extended Abstract, non reviewed, in Spanish)

Seranne, M. (1987) Evolution Tectono-Sedimentaire du Bassin de Talara (nord-ouest du Perou). *Bull. Inst. Franc. Anden*, **XVI**(3–4), 103–125. (In French).

Shepherd, G.L. & Moberly, R. (1981) Coastal structure of the continental margin, NW Peru and SW Ecuador. *Geol. Soc. Am. Mem.*, **154**, 351–391.

Silver, P.G., Russo, R.M. & Lithgow-Bertolloni, C. (1998) Coupling of South American and African plate motion and plate deformation. *Science*, **279**, 60–63.

Somoza, R. (1998) Updated Nazca (Farallon)- South America relative motions during the last 40 m.y.: implications for the mountain building in the central Andean region. *J. South Am. Earth Sci.*, **11**, 211–215.

Sosson, M., Bourgois, J. & Mercier de Lepinay, B. (1994) SeaBeam and deep-sea submersible Nautile surveys in the Chiclayo canyon off Peru: subsidence and subduction erosion of an Andean type convergent margin since Pliocene time. *Mar. Geol.*, **118**, 237–256.

Spikings, R.A., Winkler, W., Hughes, R.A. & Handler, R. (2005) Thermochronology of allochthonous terranes in Ecuador: Unravelling the accretionary and post-accretionary history of the Northern Andes. *Tectonophysics*, **399**, 195–220.

Spinelli, G.A. & Field, M.E. (2003) Evolution of continental slope gullies of the Northern California margin. *J. Sediment. Res.*, **71**(2), 237–245.

Taylor, S.R. & McLennan, S.M. (1985) *The Continental Crust: Its Composition and Evolution*. Blackwell, Oxford.

Travis, R.B. (1953) La Brea-Pariñas oil field, northwest Peru. *Am. Ass. Petrol. Geol. Bull.*, **37**, 2093–2118.

Valencia, K. & Uyen, D. (2002) Cuenca Lancones: Interpretation geologica. INGEPET, EXPR-3-KV-18. (Extended Abstract, non peer reviewed, in Spanish).

Van Wagoner, J.C., Mitchum, R.M., Campion, K.M. & Rahmanian, V.D. (1990) Siliciclastic sequence stratigraphy in well logs, cores, and outcrops. *Am. Assoc. Petrol. Geol. Methods Explor. Ser.*, **7**, 1–55.

Von Heune, R. & Scholl, D.W. (1991) Observations at convergent margin concerning sediment subduction erosion, and the growth of continental crust. *Rev. Geophys.*, **29**, 279–316.

Weiss, L. (1955) Foraminifera from the Paleocene Pale Greda formation of Peru. *J. Paleontol.*, **29**, 1–21.

Wells, R.E., Blakely, R.J., Sugiyama, Y., Scholl, D.W. & Dinterman, P.A. (2003) Basin-centered asperities in great subduction zone earthquakes-a link between slip, subsidence, and subduction erosion. *J. Geophys. Res.*, **108**(B10), 2507, doi:10.1029/2002JB002072. 1–21.

Witt, C., Bourgois, J., Michaud, F., Ordonez, M., Jimenez, N. & Sosson, M. (2006) Development of the Gulf of Guayaquil (Ecuador) during the Quaternary as an effect of the North Andean block tectonic escape. *Tectonics*, **25**, TC3017.

Manuscript received 9 April 2007; Manuscript accepted 19 October 2007.